International Journal of Plasticity 71 (2015) 32–61

Contents lists available at ScienceDirect

International Journal of Plasticity

journal homepage: www.elsevier.com/locate/ijplas

Mechanical response of low stacking fault energy Co–Ni alloys – Continuum, mesoscopic and atomic level treatments

P. Chowdhury [a], H. Sehitoglu [a,*], W. Abuzaid [a], H.J. Maier [b]

[a] Department of Mechanical Science and Engineering, University of Illinois at Urbana-Champaign, 1206 W. Green St., Urbana, IL 61801, USA

[b] Institut für Werkstoffkunde (Materials Science), Leibniz Universität Hannover, 30823 Garbsen, Germany

ARTICLE INFO

Article history:
Received 30 December 2014
Received in revised form 23 March 2015
Available online 17 April 2015

Keywords:
Density functional theory
A. Dislocations
A. Twinning
A. Strengthening mechanisms
C. Electron microscopy

ABSTRACT

Low stacking fault energy fcc alloys deform via either mechanical twinning or dislocation slip. A single crystal poses an excellent avenue to studying inherent material preference for plastic flow mechanism. This paper examines the physical process underlying the flow behavior of Co-33%Ni single crystals at continuum, mesoscale and atomic levels. Digital image correlation, electron backscatter diffraction and transmission electron microscopy permitted an in-depth analysis of the deformed microstructure. Emphasis is placed on rationalizing the experimentally discovered competing modes of plasticity from an atomistic perspective. Experimentally, predisposition for slip or twinning is observed to be specific to a given crystal orientation and loading direction (tension/compression). Particularly, flow in $\langle 111\rangle_{\text{tension}}$ and $\langle 100\rangle_{\text{compression}}$ proceeds with a single twinning system and ensuing twin-slip interactions. By contrast, dislocation slip nucleation followed by multi-system forest hardening prevails in the post-yield behavior of $\langle 123\rangle_{\text{tension}}$ and $\langle 111\rangle_{\text{compression}}$ cases. The stress-strain curves reveal that the twinning-mediated flow induces superior hardening characterized by pronouncedly serrated flow behavior. A first principle based mechanics model is proffered to account for the relative material propensity for either slip or twinning on the basis of atomic level generalized stacking/planar fault energies. The model considers the energy balance between the applied work and the total energy expenses as contributed by both continuum and atomistic effects. Upon establishing the γ surfaces from density functional theory, critical stresses for the initiation of slip, twin and post-yield twin-slip interactions are computed within a Peierls-Nabarro modeling framework. Predicted critical stress levels demonstrate reasonably good agreement with the experimentally determined critical resolved shear stresses. Concurrence of the theoretical inferences with the experimental observations is discussed in the context of the related literature.

1. Introduction

Alloying of metals has long been exploited in custom-tailoring desired mechanical properties dating as far back as to the Bronze Age (Cottrell, 2000). In modern applications, extreme operating conditions for engineering service components

* Corresponding author. Tel.: +1 217 333 4112; fax: +1 217 244 6534.
E-mail address: huseyin@illinois.edu (H. Sehitoglu).

http://dx.doi.org/10.1016/j.ijplas.2015.04.003
0749-6419/

warrant superior properties such as high strength and creep resistance. Cobalt/nickel base alloys constitute the bulk of this specialized class of materials suited for a broad thermo-mechanical loading spectrum (Davis, 2000; Smith, 1993). These materials employed in aerospace, nuclear and petrochemical industries are manufactured by adding various alloying elements to different extents so as to impart unique macro-scale characteristics. In essence, the addition of these elements invokes considerable modification to the deformation micromechanics of the respective base metals. From a solid state physics standpoint, the solute elements embedded in the matrix material contribute to the hardening effects due primarily to an atomic volume mismatch with their host lattice atoms (Neuhäuser and Schwink, 1993; Pfeiler, 2008). For the case of a binary Co–Ni alloy, the solid solution strengthening attributes would be negligible owing to the elemental volumetric ratio between Co and Ni being very close to unity. Nonetheless, the substitutional solute atoms integrated to the base metal lattice alters the fault energy landscape (Tadmor and Miller, 2011) in the alloy crystal. The adjusted electronic structure of the metallic lattice drastically affects the relative propensity of competing crystal deformation mechanisms, which occur in the form of various defect evolution (such as dislocations, stacking faults and twin boundaries). The modification in quantum bonding at the atomic substructure subtends the macroscopic operative flow mechanisms in the form of slip, twinning, twin-slip and slip–slip interaction. The gradual evolution and mutual interplays among slip and/or twinning processes in turn constitute the mechanistic origin of macroscale hardening behavior of the alloy. In view of the foregoing rationale, in the current undertaking, we are particularly interested in elucidating the relative material predilection towards slip versus twinning. In classical phenomenological considerations (Meyers et al., 2001; Miura et al., 1968; Pirouz, 1989; Venables, 1964b), the stacking fault energy (SFE) has been regarded as the most crucial material parameter in interpreting the competition between slip and twinning-dominated flow. However, recent theoretical advances (Tadmor and Bernstein, 2004; Tadmor and Hai, 2003; Van Swygenhoven et al., 2004; Warner et al., 2007) indicate that the entire γ energy surfaces (i.e. the generalized stacking/planar fault energies abbreviated as GSFE/GPFE first conceptualized by Vitek (1970) of the metallic solid solution) dictate the favored plastic flow mechanism, rather than the SFE itself. The physical interpretation of GSFE/GPFE represents the energy expenditure (per unit area) to be overcome during various degrees of rigid shear displacements between two crystals (later to be explained in more details in Sections 4.2 and 4.4). These γ energy landscapes are reported to be strong functions of the material electronic structure (Ogata et al., 2002), which can be resolved by quantum mechanical methods (Dreizler and Engel, 2011). In the last decade, significant advancement in computational material science has prompted major strides in understanding the non-continuum effects of slip/twinning processes, establishing the physical rationale behind observed plastic mechanism (McDowell, 2010; Shin and Carter, 2014; Xiong et al., 2015). Evidently, these important discoveries entail a revisit to the classical modeling endeavors, and, thereby, incorporation of the most contemporary knowledge of the underlying atomistics into deformation theory. The present research is aimed at addressing the long-standing question of theorizing the preferred mode of plastic deformation via slip or mechanical twinning on a physical basis, principally noting their respective atomic level fault energetics. We build on the foundation laid by classical and modern plasticity theories, and forward a model accompanied by extensive experimental analyses. We study the experimental stress-strain behavior and the associated deformation features of a representative low stacking fault energy material at the microstructure level.

Within the current scope, we have selected single crystals made from a Co-33%Ni alloy. Early literature (Beeston et al., 1968; Gallagher, 1970; Howie and Swann, 1961) reports that the polycrystalline Co-33%Ni alloy possess a considerably low stacking fault energy ($\approx$20 mJ/m^2), and a face centered cubic (fcc) crystal structure. Single crystals offer a superior understanding of the metallic deformation mechanics by circumventing the effects of grain boundaries and texture associated with polycrystalline materials (M'Guil et al., 2014; Xiao et al., 2015). The choice of this particular binary composition of Co–Ni is especially advantageous, in that this material is reportedly predisposed to plastic deformation via mechanical twinning at room temperature (Remy, 1978). Moreover, we note that a judicious selection of the Co–33%Ni single crystal orientation and loading direction (tension or compression) culminates in the plasticity proceeding preferentially via either dislocation slip or mechanical twinning. Consequently, it facilitates characterizing the governing variables pertaining to the preferred deformation mode both on experimental and theoretical grounds as noted in the literature of low SFE materials (Egner and Skoczeń, 2010; Paul et al., 2007; Salehinia and Bahr, 2014). The current analysis of the Co–33%Ni alloy serves to be representative of low SFE fcc alloys, and hence can pave the way for extending the inferences reached in this work to similar classes of materials.

In early literature (Meyers et al., 2001; Miura et al., 1968; Paul et al., 2009; Pirouz, 1989; Venables, 1964b), lowering of the SFE in fcc metals and alloys has been correlated with an increased inclination to deformation by a mix of planar/wavy slip and deformation twinning. The strain hardening response would be pronouncedly altered subjected to the activation of slip or twinning upon yielding. Typically, twinning-dominated strain hardening is manifested in the form of a serrated stress-strain curve (Christian and Mahajan, 1995; Paul et al., 2009). Experimental observations suggest that the preferred plastic mechanism would be a strong function of the loading direction and crystallographic orientation (Hong et al., 2009), provided the respective critical stresses (which are material properties) are similar. Depending on compressive or tensile load along a certain crystallographic orientation, different levels of shear stresses would be resolved on various slip and twinning systems as per the Schmid law. On account of the maximum Schmid factor, a specific loading configuration would trigger either slip or twin nucleation accordingly. In slip-mediated plasticity, low stacking fault energy would promote splitting of full dislocations into Shockley partials bound by a stacking fault. Early literature notes that the mechanistic process of deformation twin nucleation and migration processes is fundamentally founded on the collective glide pattern of Shockley partial dislocations (Blewitt et al., 1957; Christian and Mahajan, 1995; Jin and Bieler, 1995; Liu et al., 2012, 2014; Müllner and Romanov, 2000;

Venables, 1964a). The successive passage of Shockley partials on consecutive slip planes amounts to the mechanical twinning phenomenon. Therefore, in classical modeling undertakings, twin nucleation and migration processes are generally treated by considering the elastic interaction effects among the twinning partial dislocations (Christian and Mahajan, 1995; Cooper, 1965). A more comprehensive account of the classical twinning models is discussed in Section 5.2 of this paper. In summary, the previous models in the literature are mostly empirical (requiring fitting parameters), and hence cannot predict the critical stress magnitudes of various flow mechanisms from physical considerations (e.g. twin or slip nucleation, twin-slip interaction etc.). Most importantly, the evolution of fault energetics related with the shearing of the discrete crystal lattice (Van Swygenhoven et al., 2004; Vitek, 1970) accompanying slip/twinning processes has not been utilized in quantifying the macro-scale flow stresses. Essentially, the non-continuum nature of the metallic crystal at the atomic level necessitates overcoming periodic resistance forces, i.e. the so-called Peierls barrier during the slip or twinning process. The periodic energy-displacement correlation associated with slip- and twinning-induced shearing at the atomic level can be correctly outlined by the so-called γ surfaces i.e. generalized stacking fault energy (GSFE) and generalized planar fault energy (GPFE) profiles. However, these γ surfaces can only be quantified theoretically with the knowledge of the underlying electronic nature of the specific metal or alloy system. With the advent of modern quantum mechanical simulation tools such as density functional theory (DFT) (Dreizler and Engel, 2011), one can precisely account for the electron bonding effects from first principles, thereby permitting accurate computation of the GSFE/GPFE levels. These γ surfaces provide an ab-initio energetic perspective into the material predilection for the operative plasticity. Furthermore, they constitute essential ingredients in the recipe of predicting critical stresses for slip and twin nucleation within a Peierls-Nabarro modeling framework.

Fig. 1 illustrates an overview of the scale and structure of the current methodology directed at addressing the deformation mechanisms of Co–33%Ni. We adopt a bottom-up approach comprising electronic properties at the atomic lengthscale, the onset of defect dynamics at the mesoscale, and continuum level critical flow stresses. At the continuum scale, uniaxial tension and compression experiments are conducted on single crystals loaded along ⟨111⟩, ⟨123⟩ and ⟨001⟩ directions. The loading orientations are selected on the basis of prompting the material to deform via twinning or slip. Critical resolved shear stresses for dislocation slip and mechanical twin nucleation is extracted from the stress-strain curves with the aid of Schmid law. In-situ digital image correlations (DIC) analysis is used to study the nature of the active plastic systems providing a measure of

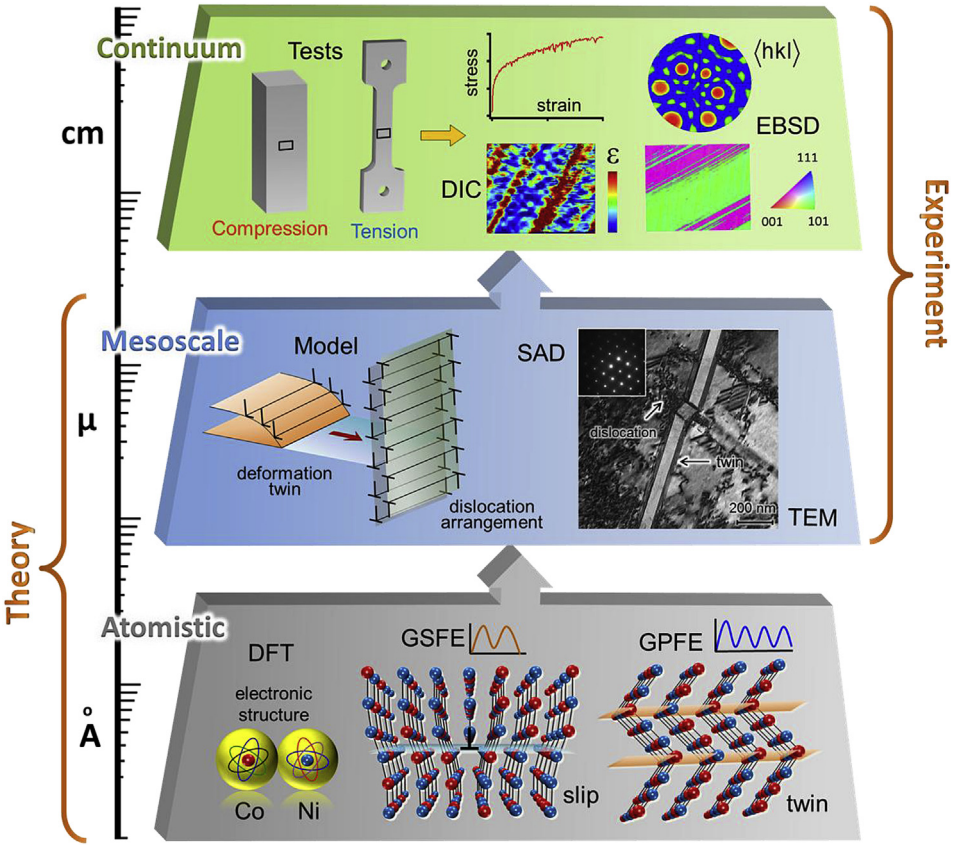

Fig. 1. A schematic illustrating the lengthscale of the current study. Tension/compression experimental data are analyzed via DIC and EBSD methods at continuum level. Mesoscale considerations include extensive microstructure study via TEM and SAD accompanied by modeling efforts. At atomic level, GSFE/GPFE curves are computed from the electronic structure of Co–Ni alloys using DFT.

the strain localization levels. In addition, ex-situ electron backscatter diffraction (EBSD) scans are performed so as to reveal local misorientations associated with twinning. Extensive transmission electron microscopy (TEM) conducted ex-situ in and around the localized strain bands permits a detailed insight into the flow mechanism for the individual loading cases. Complementary selected area diffraction (SAD) patterns in conjunction with the TEM images confirm the presence of local material reorientation (i.e. twinning-induced) by revealing twin diffraction spots. At the mesoscale, we model critical resolved shear stresses for slip and twinning (i.e. demarcating the onset of plasticity) as well as the critical stress level indicating the onset of twin-slip interaction (i.e. second stage of hardening following the initial plasticity). We utilize a Peierls-Nabarro modeling framework, which accounts for continuum elastic theory of dislocation interaction and non-continuum γ surfaces. The central premise of the Peierls-Nabarro model requires generalized stacking fault energy (GSFE) and generalized planar fault energy (GPFE) landscapes, to be considered as essential constituents. To that end, density functional theory (DFT) simulations are employed to compute the ab-initio γ surfaces based on the electronic structure of the Co-33%Ni fcc solid solution.

The current study, based on the behavior of Co-33%Ni as a representative material, can be deemed as a necessary revisit to the fundamental deformation theory related to the low SFE fcc alloys. Reinforced with sufficient experimental evidence, we propose to accommodate the quantum mechanical contributions of material deformation to the classical continuum context addressed in recent literature (Clayton, 2010a; Clayton and Knap, 2013). As a result, we derive the critical flow stress predictions free of empirical constants.

2. Methods

2.1. Material preparation and monotonic experiments

Single crystal specimens of Co−33%Ni were fabricated using the Bridgman technique in an inert Helium atmosphere. Room temperature tension and compression experiments were conducted using 1.5 mm × 3 mm × 10 mm (dog-bone) and 4 mm × 4 mm × 10 mm specimens (thickness x width x gage-length), respectively, at a strain-rate of 5×10^{-5} s^{-1}. Prior to the tests, all the specimens were solutionized at a constant temperature of 900 °C for one hour and then quenched by room temperature water. The loading axes for the tension samples were aligned along ⟨123⟩ and ⟨111⟩ crystallographic directions, and the compression samples along ⟨001⟩ and ⟨111⟩. These orientations were verified by electron backscatter diffraction (EBSD) analyses. Each set of loading (compressive or tensile) and crystal orientation case was investigated with multiple companion experiments (up to four tests per each case) to ensure the repeatability of the stress-strain trends, and hence statistically reduce the experimental error levels. The samples were loaded in a servo-hydraulic load frame where strain levels were measured using a miniature extensometer and stress levels with a load cell. Post-deformation microstructure is then studied ex-situ with transmission electron microscopy (TEM).

2.2. Digital image correlation (DIC)

DIC is an experimental visualization method that utilizes the distinction between a reference and a modified speckle pattern pre-deposited on the specimen surface in question. The surfaces of the specimens were polished to a mirror finish for DIC analysis. An adherent layer of black paint was airbrushed onto the polished surfaces to create a fine speckle pattern thereon. An IMI model IMB-202FT CCD digital camera (1600 pixel × 1200 pixel) was used to capture high resolution images for the reference state and deformed state of the surface under study. In-situ DIC measurement was utilized to identify the strain localization contour plots in real time at various levels of macroscale deformation. In addition, higher resolution ex-situ DIC was performed in order to identify the number of active plastic systems as well as distinguish between various local strain bands (slip- and twinning-induced).

2.3. Density functional theory (DFT)

The DFT is a quantum mechanical simulation method based on the Schrödinger's equation, where the interatomic bonding forces are determined by the valence electrons. Two primary assumptions of the DFT based modeling of the deformation are that: (a) the plastic deformation is equivalent to the permanent movement of atomic nuclei, which are bonded together by sharing electronic clouds (also known as the Born-Oppenheimer approximation), and (b) inter-nuclei forces are solved in terms of the electronic densities (instead of direct solutions of wave functions) to achieve numerical feasibility. For example, the slip of material creates a permanent atomic displacement equal to the Burgers vector. Using DFT methods, one can solve for the associated free energy differential (i.e. the energy cost to create such displacement). Hence, the GSFE and GPFE curves were constructed by computing the energy differential between the bulk (E_{bulk}) and sheared ($E_{sheared}$) crystal normalized by the shear area (A) as in Equation (1) after Vitek (Vitek, 1970).

$$\gamma = \frac{E_{sheared} - E_{bulk}}{A} \tag{1}$$

The convergence of the γ energy levels was ensured with respect to the simulation supercell size (i.e. number of layers in x, y and z directions). Three dimensional periodic boundary conditions were enforced on the supercell, which eliminates the effects of free surface energy, thereby simulating a system of bulk material. Shear displacement is applied along the x direction (corresponding to the ⟨112⟩ crystallographic direction) on the y plane (i.e. {111} slip plane), which generated corresponding shear forces. It was ensured that no traction existed except for the designated shears. For the post-processing of simulation data, the atomic configuration viewer, VMD (Visual Molecular Dynamics) (Humphrey et al., 1996) was used.

For the current DFT calculations, we used the commercial quantum simulation software - *Vienna Ab initio Simulation Package* (VASP) (Kresse and Furthmüller, 1996) to create the solid solution of Co-33%Ni. Upon constructing the Co–Ni fcc crystal structure, the *conjugate gradient* method was used to iteratively minimize the total energy of the overall crystal structure, and the atomic positions were updated accordingly. During the iteration, an acceptance criterion adjusts the new atomic positions, conjugate to the previous ones that follow the direction of the steepest descent on the inter-atomic energy profile (which is established by solving for the valence electron densities). Inherent in DFT assumptions are the charged nature of the atomic nuclei (positively charged) and the surrounding electronic cloud (negatively charged). To model the electrostatic interactions among the nuclei and electrons, the *projector augmented wave method* was used. During deformation, electron movements are "correlated" due to their mutual Coulombic interactions (the so-called correlation effects); to make each electronic energy state unique (as dictated by *Pauli's exclusion principle*), the densities of two electrons have to be antisymmetric upon switching positions (the so-called exchange effects). The exchange-correlation energies were computed using the *generalized gradient approximation* (Kresse and Hafner, 1993). The DFT based electronic solutions are conducted in reciprocal space by creating a meshed Brillouin zone. In the current work, the Brillouin zone is constructed as a $12 \times 12 \times 12$ mesh size (using Monkhorst Pack k-point with an energy cut-off of 300 eV). Spin polarized conditions were enforced on the electrons, which ensures the ferromagnetism of the elemental Co and Ni. For a fundamental discussion of the quantum modeling of materials, the readers are also referred to (Tadmor and Miller, 2011).

3. Experimental results

3.1. Stress-strain behavior

Fig. 2(a) and (b) report the experimental resolved stress-strain levels of Co–33%Ni single crystals loaded along four different crystallographic directions. Resolved shear stresses (nominal) on the activated systems for respective curves have been plotted against the resolved shear strains. Depending upon the operative mode of plasticity, the global stress-strain levels are resolved on the maximum Schmid factor slip or twinning systems. These plots illustrate the differences in single crystal plastic flow response as a function of the crystal orientation as well as the loading direction. A careful examination of the post-deformation microstructure (with the aid of extensive TEM and EBSD analyses, to be discussed in Section 3.2) suggests the existence of different plastic flow mechanisms for the individual cases. For ⟨111⟩ tension and ⟨100⟩ compression, flow mechanism has been found to be dominated by deformation twinning. On the other hand, ⟨123⟩ tension and ⟨111⟩ compression deform plastically due primarily to dislocation slip.

In Fig. 2(a), the stress-strain response in ⟨111⟩ tension is characterized by highly serrated flow. By contrast, the flow stress under ⟨123⟩ tension appears rather uniform. The serrated plastic stress-strain for the ⟨111⟩ tension and ⟨001⟩ compression indicates twinning-based hardening behavior. On the other hand, the ⟨123⟩ tension and ⟨111⟩ compression curve is noticeably indicative of a dislocation slip-induced flow mechanism. The tensile yield stresses for ⟨111⟩ and ⟨123⟩ tension (0.1% offset) have been found to be 27 ± 5 MPa and 15 ± 1.5 MPa, respectively. These yield stresses denote the critical resolved shear stresses (τ_{CRSS}) for twin or slip nucleation for the Co–33%Ni alloy. The τ_{CRSS} is considered a material property independent of loading direction and orientation. Under compression as in Fig. 2(b), the ⟨001⟩ single crystal shows a yield stress level of 26 ± 3 MPa whereas that of the ⟨111⟩ case is determined to be 16 ± 1.2 MPa. These stress values represent the critical resolved shear stresses for twin and slip nucleation respectively, which are consistent with the tension results. We note that multiple experiments are conducted to ensure the repeatability of the stress-strain trends as indicated by the error bars in Fig. 2(a) and (b). Therefore, the critical resolved shear stresses extracted from these stress-strain curves represent the statistical average values over multiple measurements. The horizontal arrows adjacent to each curve on the right hand side indicate that the experiments were continued to higher strain levels (than shown). We note that the rest of the stress-strain response in Fig. 2(a) and (b) are mere continuation of the trend as currently presented. It is our objective in this work to study the very initial stage of the plasticity, i.e. the phenomena such as onset of slip, twinning, twin-slip interaction etc. The subsequent modeling is directed at predicting the foregoing critical stresses to initiate various plasticity mechanisms.

A summary of the foregoing findings is presented in Table 1. In addition, critical resolved stress for the activated plastic flow mechanism in polycrystalline Co-33%Ni has been studied (discussed in Appendix A).

3.2. Microstructure

3.2.1. ⟨111⟩ *Tension*

Fig. 3(a) illustrates the in-situ DIC local strain contour on the {101} surface of a single crystal sample loaded along ⟨111⟩ in tension. The plot shows the residual local strain (normal and not shear) after deformation. The localization of strain in bands is associated with the activation of a particular slip/twin system. To accurately identify these strain bands observed in this case

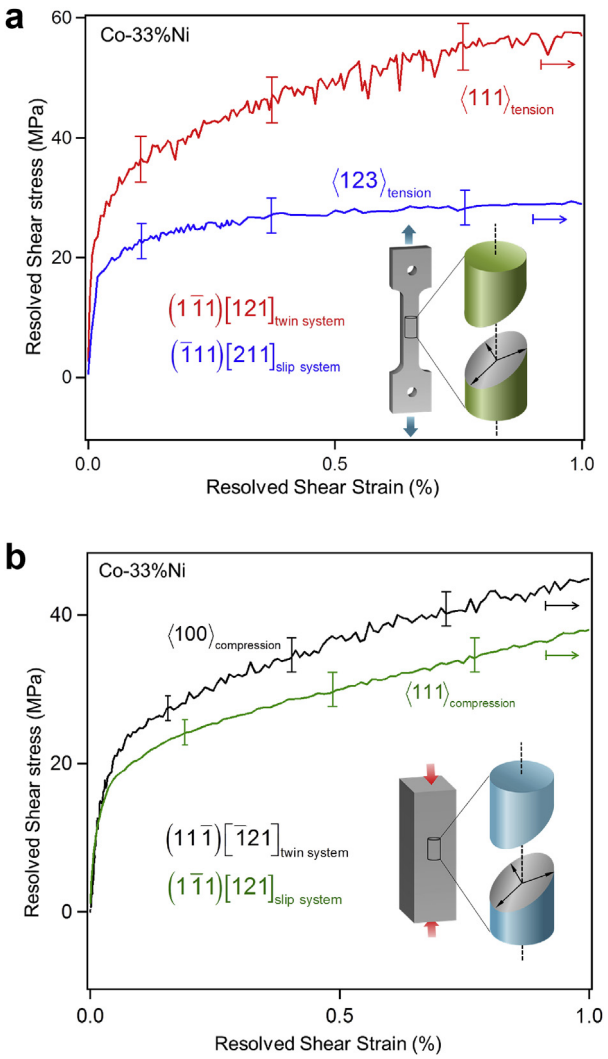

Fig. 2. (a) – Shear stress-strain for ⟨111⟩ and ⟨123⟩ tension cases resolved onto (1$\bar{1}$1)[121] and ($\bar{1}$11)[211]. The error bars represent multiple experiments. The arrow pointing to the right indicates that experiments were continued at higher stains. (b) – Shear stress-strain for ⟨100⟩ and ⟨111⟩ compression cases resolved onto (11$\bar{1}$)[$\bar{1}$21] and (1$\bar{1}$1)[121] twin and slip system respectively.

Table 1
Summary of Schmid factor analysis and experimental determination of critical resolved shear stress (CRSS).

Cases	Maximum Schmid factor				Observed system(s) activated	Observed flow mechanism	Experimental τ_{CRSS} (MPa)
	Slip	Twin	Partials				
			Leading	Trailing			
⟨111⟩ tension	0.27	0.31	0.31	0.16	(1$\bar{1}$1)[121]	Twinning	27 ± 5
⟨123⟩ tension	0.47	0.47	0.47	0.34	($\bar{1}$11)[211]	Slip	15 ± 1.5
⟨111⟩ compression	0.28	0.16	0.16	0.31	(1$\bar{1}$1)[121] (11$\bar{1}$)[$\bar{1}$21]	Slip	16 ± 1.2
⟨100⟩ compression	0.41	0.47	0.47	0.24	(11$\bar{1}$)[$\bar{1}$21]	Twinning	26 ± 3

(whether caused by either slip or twinning), EBSD scans on the same deformed surface were conducted as presented in Fig. 3(b) and (c). Inverse pole figures in Fig. 3(b) indicate significant crystal misorientations in the deformed crystal. The presence of more than one orientation is also noticeable in the distribution of ⟨100⟩ and ⟨110⟩ poles. In Fig. 3(c), an EBSD map of the {101} surface identifies the DIC-observed shear bands as induced by local crystal misorientation. Based on the maximum Schmid factor, this twinning system has been identified as (1$\bar{1}$1)[121]. The misorientation of the twin with respect to the matrix material has been determined to be approximately 60° from the EBSD data. TEM micrographs sampled from the bulk of the crystal in Fig. 4(a)–(e) further attest to the fact that the shear bands are caused by deformation twinning.

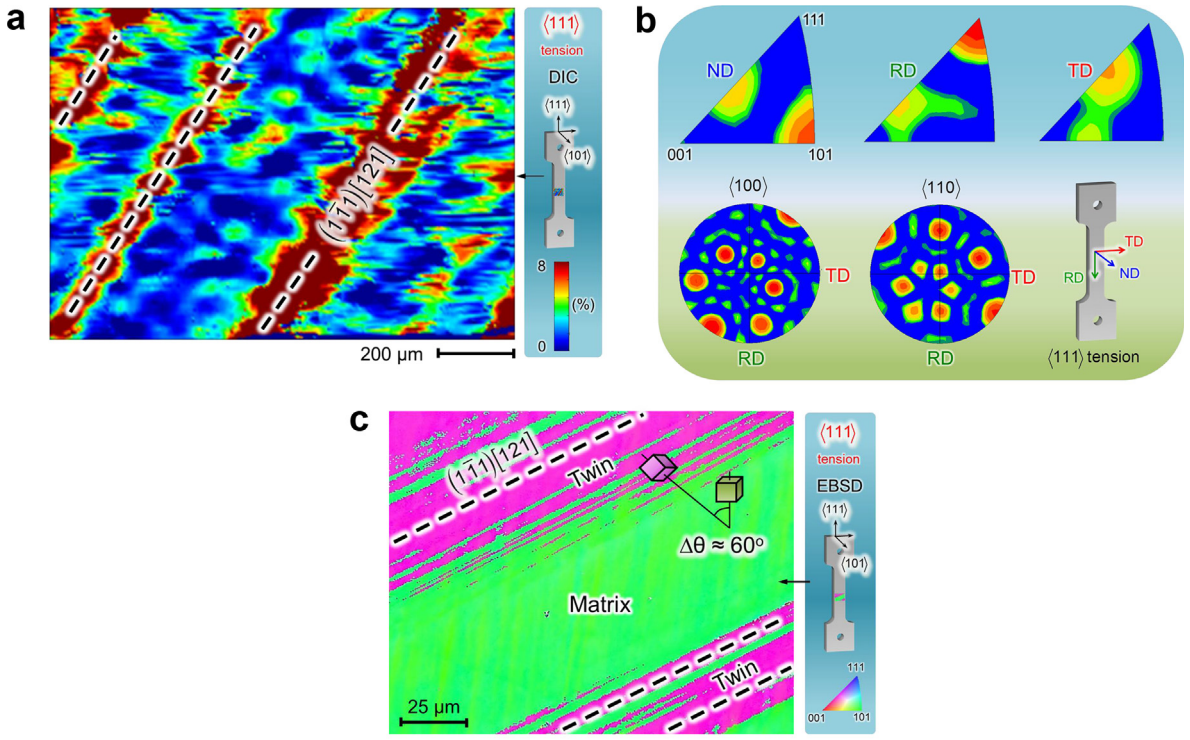

Fig. 3. (a) – Ex-situ DIC local strain contour on the {101} surface of a single crystal sample loaded along ⟨111⟩ in tension. (b) – EBSD data for ⟨111⟩ tension are presented in the form of inverse pole figures (upper row) and pole figures showing the distributions of ⟨100⟩ and ⟨110⟩ crystallographic directions. (c) - Another presentation of EBSD data from the {101} surface of the specimen in tension along ⟨111⟩ direction. The presence of a 60° misorientation between the matrix material and strain bands substantiates the occurrence of deformation twinning.

The TEM image in Fig. 4(a) shows the prevalence of nano-scale parallel mechanical twins. The SAD patterns in the inset further testify to the presence of twins in the sampled material. Another magnified view of the deformed area is presented in Fig. 4(b). Parallel deformation twins are distinctly visible in the micrograph. The corresponding SAD pattern confirms the twin reflections. Fig. 4(c) illustrates a number of fine twins advancing through a forest of stacking faults (binding partial dislocations at both ends). An example of a propagating mechanical twin interacting with a dislocation arrangement is presented in Fig. 4(d). A deformation twin appears to have created a kink upon interacting with a pre-existent local dislocation arrangement. Further evidence of twin-slip interactions can be noted in Fig. 4(e). A representative deformed microstructure in the close proximity of twinning bands is shown in Fig. 4(e).

The analyses of these micrographs indicate that the flow behavior of the single crystals deformed in ⟨111⟩ tension is characterized by mechanical twinning as the primary deformation mode. Secondary strain hardening effects can be attributed to the interaction between the propagating mechanical twin and the local dislocation arrangements as well as classical forest hardening among dislocations themselves. However, no evidence of twin–twin interaction has been found from the DIC and TEM investigations. Upon straining the material to a level as high as 7%, the deformed surface morphology indicates no major variation in the observed plastic flow mechanism. The preferred deformation mode through a broad range of strain has been found to be consistently dominated by parallel non-interacting deformation twin nucleation followed by twin migration, which is influenced by twin-slip interaction.

3.2.2. ⟨123⟩ *Tension*

Fig. 5 illustrates an EBSD scan of a {101} surface of a Co–33%Ni single crystal sample loaded along ⟨123⟩ in tension to a strain level of 60%. It follows from the EBSD that a uniform orientation exists throughout the deformed surface (as opposed to the ⟨111⟩ case in Fig. 3(c), where twinning causes considerable local misorientation in the form of bands). The EBSD result demonstrates no presence of local misorientation with respect to the matrix material (which confirms the nonexistence of twinning for ⟨123⟩ tension). Furthermore, the TEM evidences as presented in Fig. 6(a)–(e) reveal extensive slip activities (with no twinning). These images support the EBSD results concluding that deformation is slip-mediated for the single crystal in ⟨123⟩ tension. We note that the slip predominantly occurs as $a/6\langle 112\rangle$ type.

The micrograph in Fig. 6(a) illustrates an instance of microscopic slip band (MSB) formation due to dislocation slip on parallel planes along a single slip system. Entanglement of dislocations interacting with the slip band can be noticed in the inter-band regions. In Fig. 6(b), a magnified view of the deformation morphology near the band shows the entanglement of dislocations in the neighborhood of the band structure. Fig. 6(c) shows further evidence of entangled dislocations. These

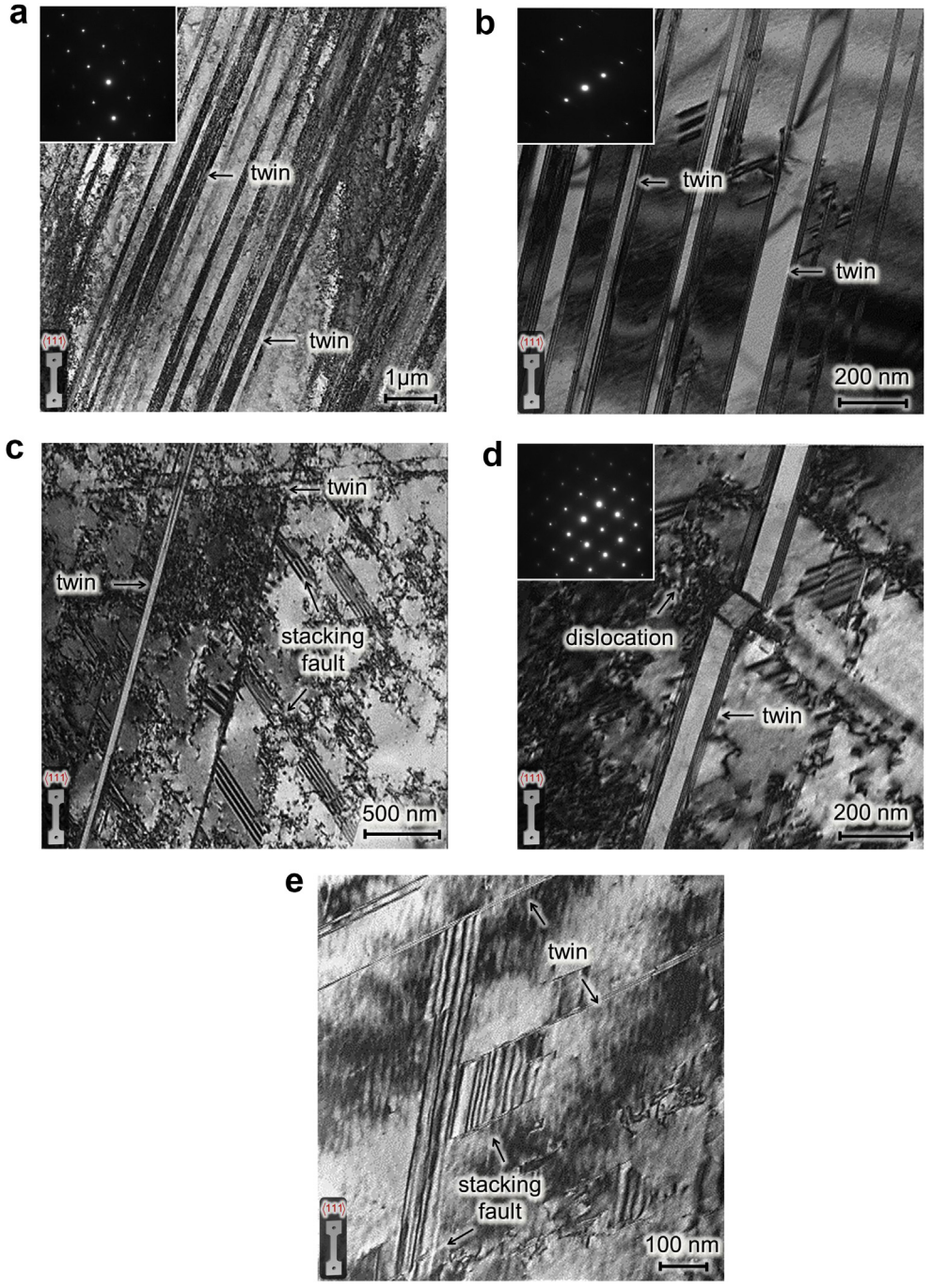

Fig. 4. (a) – TEM and SAD for ⟨111⟩ tension demonstrating the deformation twins. (b) – A magnified view of twins with the corresponding SAD spots (in ⟨111⟩ tension). (c) – Further evidence of twinning in ⟨111⟩ tension along with the presence of stacking faults. (d) – An example of a propagating mechanical twin interacting with a dislocation arrangement (in ⟨111⟩ tension).(e) – Evidence of twin-stacking fault intersections (under ⟨111⟩ tension).

entangled dislocations dissociated into partial dislocations bound by stacking faults, the evidence of which is shown in Fig. 6(d) and (e). Splitting of full dislocation arrangements into partials, thereby creating co-planar stacking faults, can be seen in Fig. 6(d). Additionally, parallel fine stacking faults at low applied strain level are visible in Fig. 6(e).

3.2.3. ⟨111⟩ Compression

Fig. 7(a) illustrates the in-situ DIC local strain distribution on the {101} surface of Co-33%Ni single crystal compressed along the ⟨111⟩ crystallographic orientation. Two systems of intersecting strain bands can be observed. To understand

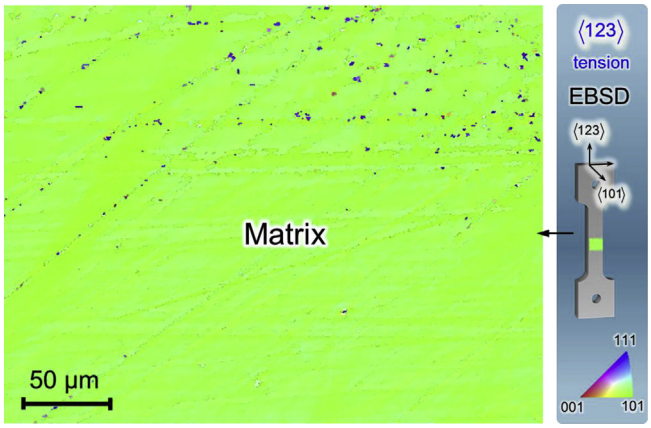

Fig. 5. EBSD scan of a {101} surface of a Co-33%Ni single crystal sample loaded along ⟨123⟩ in tension to a strain level of 60%.

whether these strain bands are due to slip or twinning, we have conducted EBSD scans on the same surface as presented in Fig. 7(b). The EBSD result reveals no local crystal misorientation (as opposed to the 60° misorientation bands visible in the ⟨111⟩ tension case). This observation dismisses any occurrence of twinning associated with the strain bands identified via DIC. On the basis of the maximum Schmid factor, these two systems are identified as the $(1\bar{1}1)[121]$ and $(11\bar{1})[\bar{1}21]$ slip systems. The TEM micrographs in Fig. 8(a)–(e) provide more in-depth views into the operative plastic flow mechanism.

In Fig. 8(a), intersecting stacking faults from two different systems are visible near a macroscopic dislocation band formed along a third system. Fig. 8(b) shows a magnified view of the same area, providing a clear visualization of the faults interlocked with each other. Another deformed area is reported in Fig. 8(c), depicting the presence of parallel stacking faults as a consequence of splitting of full dislocations into Shockley partials. Fig. 8(d) and (e) demonstrates further evidence of the prevalence of stacking faults. These TEM findings confirm the widespread participation of extended dislocations as the material continues to deform plastically to higher strain levels.

3.2.4. ⟨100⟩ Compression

For the ⟨001⟩ compression samples, an in-situ DIC strain contour on the {001} surface is presented in Fig. 9(a) at an applied (global) strain level of about 6%. Parallel non interacting strain bands are distinctly visible. These bands are identified as the $(11\bar{1})[\bar{1}21]$ slip system (corresponding to the maximum Schmid factor). Fig. 9(b) presents the EBSD analysis of the {001} surface of the deformed specimen. The EBSD data confirm that there exists a 60° (approximately) misorientation between the matrix and the strain band (i.e. twins) as illustrated with the rotated cubes. This observation attests to the occurrence of twining associated with the strain localizations seen in the DIC image. In Fig. 10(a) through Fig. 10(e), the TEM micrographs provide further evidence of twinning in the deformation of Co–33%Ni single crystals in ⟨001⟩ compression.

Fig. 10(a) reports the presence of mechanical twins in the deformed single crystal. Some stacking faults are also visible in the close neighborhood of the twin. The inset SAD patterns show the twin diffraction spots as a result of deformation-induced crystal reorientation, thereby confirming the presence of twinning in the probed area. Another part of the deformed crystal as in Fig. 10(b) showed twins, stacking faults and grouped dislocation. Fig. 10(c) reveals fine twins as demonstrated by the corresponding SAD pattern in the inset. In Fig. 10(d), a mechanical twin propagating through what appears to be an entanglement of grouped dislocations is clearly visible. Finally, Fig. 10(e) illustrates an instance of twin advancement through a forest of dislocation entanglements.

4. Theoretical results

4.1. DFT simulation of Co-33%Ni solid solution

Fig. 11 shows the potential energy per atom as a function of lattice constant, $a_{Co\text{-}Ni}$, of the Co-33%Ni solid solution as calculated from density functional theory (DFT) simulations. The lattice constant of the alloy is determined by considering the magnitude of $a_{Co\text{-}Ni}$ corresponding to the minimum per-atom energy as highlighted with a solid circle in Fig. 11. The basis of the crystal lattice is considered fcc-structured. The lattice constant $a_{Co\text{-}Ni}$ for Co-33%Ni alloy has been determined to be 3.521 $\mathring{A}$ with the per-atom energy level of −5.4438 eV (electron volt). The current value of the lattice constant is in good agreement with the experimental value of 3.52 Å of the same composition (Nishizawa and Ishida, 1983). The inset illustrates the primitive unit cell of the Co–Ni alloy. In view of the fact that Co–Ni is a disordered alloy i.e. with no long or short range atomic order, the solute atoms (Ni) are distributed randomly in the Co–Ni substitutional solid solution matrix. Upon establishing the lattice constant of the binary alloy, we simulate rigid shear of two crystal blocks consisting of discrete atoms in to order to construct the associated planar fault energy profile.

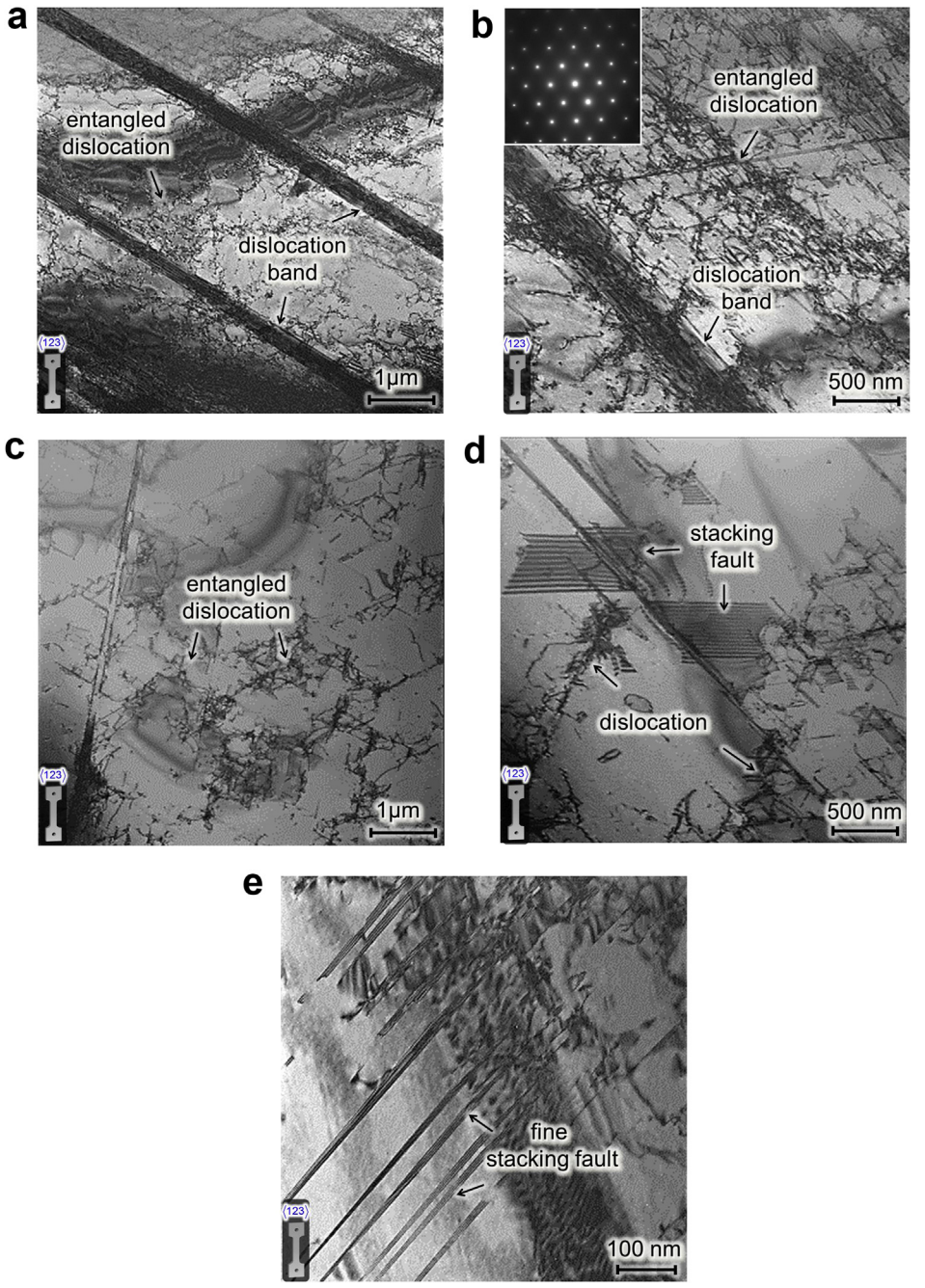

Fig. 6. (a) – Microscopic slip band (MSB) formation due to dislocation slip on parallel planes along a single slip system (in ⟨123⟩ tension). (b) – A magnified view of Fig. 6(a) demonstrates dislocation entanglement in the vicinity of the microscopic strain band (in ⟨123⟩ tension). (c) – Further evidence of entangled dislocations (under ⟨123⟩ tension). (d) – Formation of stacking faults as a result of splitting of full dislocations (in ⟨123⟩ tension). (e) – Fine stacking faults are observed (in ⟨123⟩ tension).

Fig. 12(a) shows a planar cutaway view of the close-packed (111) slip plane in the Co-33%Ni alloy. Slip or twinning phenomenon causes permanent shear displacement of the atomic lattice on the slip/twinning plane and slip/twinning direction as denoted by the associated Burgers vectors, $\vec{b}$. For a fcc lattice, partial dislocation slip as well as deformation twinning occur on the {111} family of planes along any of the ⟨112⟩ family of crystallographic directions. Hence, to profile the shear-induced energy-displacement landscape for a specific slip/twin system, two crystal blocks with adjoining interface on the (111) slip (highlighted in green and gray) were rigidly displaced along the [121] direction in the DFT simulations. Fig. 12(b) illustrates an example of the resultant structure as a consequence of shearing of the two blocks by a displacement of $|\vec{b}|$ along

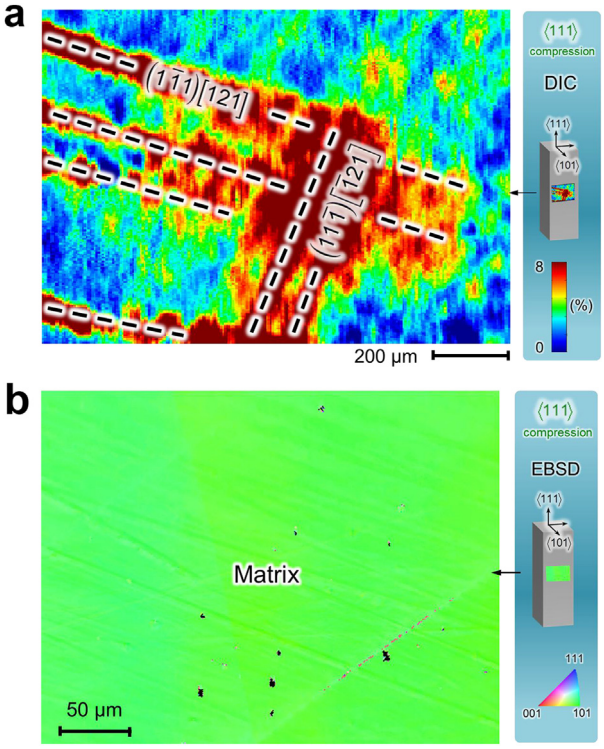

Fig. 7. (a) – In-situ DIC local strain distribution on the {101} surface under ⟨111⟩ compression demonstrating two systems of intersecting strain bands. (b) – EBSD scan of the {101} surface showing the existence of a uniform crystal orientation upon 3% global strain (under ⟨111⟩ compression).

the vector, $\vec{u}_{ab} = \vec{b} = a_{Co-Ni}/6[112]$. The lattice structure represents a discontinuation from the regular fcc stacking, i.e. a stacking fault in the fcc lattice (as highlighted with the dark gray area and yellow line). GSFE and GPFE plots were constructed by computing the entire energy profile in course of rigid shearing as a function of the displacement as presented in Figs. 13 and 15, respectively.

4.2. Generalized stacking fault energy (GSFE)

Fig. 13 reports the DFT-computed GSFE of the Co-33%Ni solid solution. The inset diagrams illustrate the atomic configurations corresponding to the various energy levels on the curve. Starting with an initial perfect fcc stacking, shear displacement along the [121] direction (a→b) by $|\vec{u}_{ab}| = |\vec{b}|$ results in a stacking fault configuration. The energy barrier to create the stacking fault (i.e. the unstable stacking fault energy, γ_{us}) has been found to be about 205 mJ/m^2. The intrinsic stacking fault energy, γ_{isf}, is calculated to be 20 mJ/m^2, which is in agreement with the experimentally determined value (Beeston et al., 1968; Gallagher, 1970; Howie and Swann, 1961). The lattice with the stacking fault, upon shearing by an equal displacement along the [$\bar{1}$12] direction (b→c), reverts back to the perfect fcc lattice. The thus-generated γ surface represents the atomic level periodic energy profile associated with an extended dislocation, i.e. two partials bound by a stacking fault in-between. The γ energy consideration is used as an important constituent in calculating the corresponding Peierls stress, τ^{slip}_{CRSS}.

4.3. Critical resolved shear stress for slip nucleation τ^{slip}_{CRSS}

The Peierls–Nabarro model provides the theoretical framework for predicting crystal impedance to slip. According to the Peierls-Nabarro theory, the introduction of a dislocation in a perfect crystal requires overcoming two different types of energy expenses – elastic (long-ranged) and misfit (short-ranged) energies (Hirth and Lothe, 1982).

The elastic energy expense originates from the resistance to the stretching of atomic bonds surrounding the dislocation core. The elastic displacements of the atoms are represented by the so-called disregistry function, f(x), upon insertion of an extra half-plane of atoms creating the dislocation (Hirth and Lothe, 1982). On the other hand, the aforementioned misfit energy cost arises from the dislocation glide on a particular slip plane along a slip direction. The GSFE serves to capture the atomistic energy expenditure in the slip-induced shear of the discrete lattice. The misfit energy can be obtained by calculating the area underneath the GSFE curve (hence, we denote it as the "E_{GSFE}" in the following discussion). In order to compute the Peierls stress i.e. lattice frictional resistance, one needs to quantify both the disregistry and the misfit contributions.

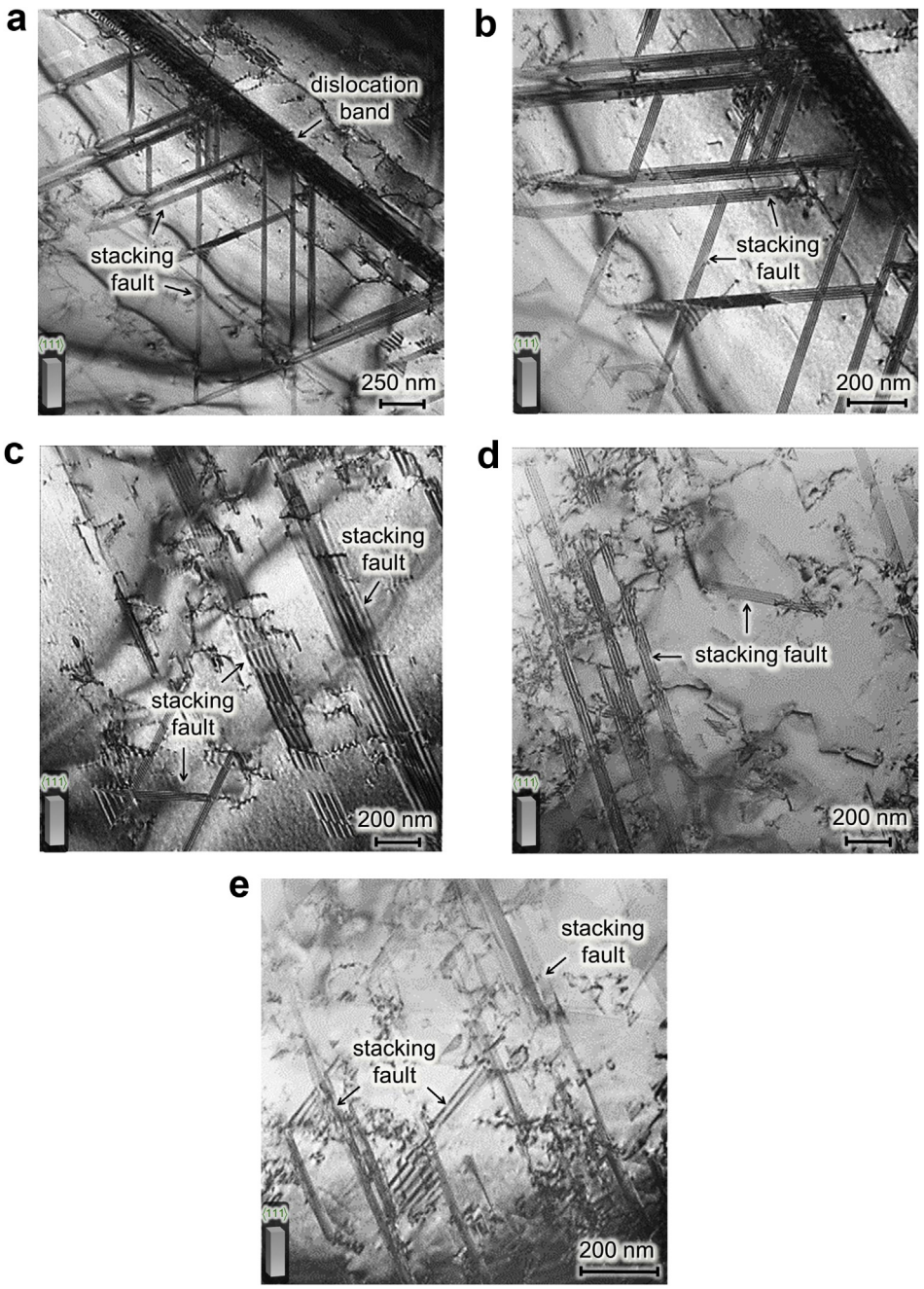

Fig. 8. (a) – Intersecting stacking faults from two different systems can be seen close to a dislocation band formed along a third slip system (in ⟨111⟩ compression). (b) – A magnified view of Fig. 8(a), providing a clear depiction of the faults interlocked with each other (⟨111⟩ compression). (c) – Parallel stacking faults as a consequence of splitting of full dislocations into Shockley partials (⟨111⟩ compression). (d) – Presence of stacking faults is visible (⟨111⟩ compression). (e) – Further evidence of stacking faults (⟨111⟩ compression).

Fig. 14 illustrates the physical significance of the disregistry function, f(x), for the case of a full dislocation (i.e. no partials). The function f(x) captures the horizontal displacement differential of the atoms (before and after the occurrence of slip) across the slip plane. The analytical solution of f(x) is obtained by balancing the total elastic force with the periodic restoring force of the lattice.

For any extended dislocation with a partial separation distance, d, the disregistry function f(x − d) is given by Equation (2) (Schoeck, 1994, 2005).

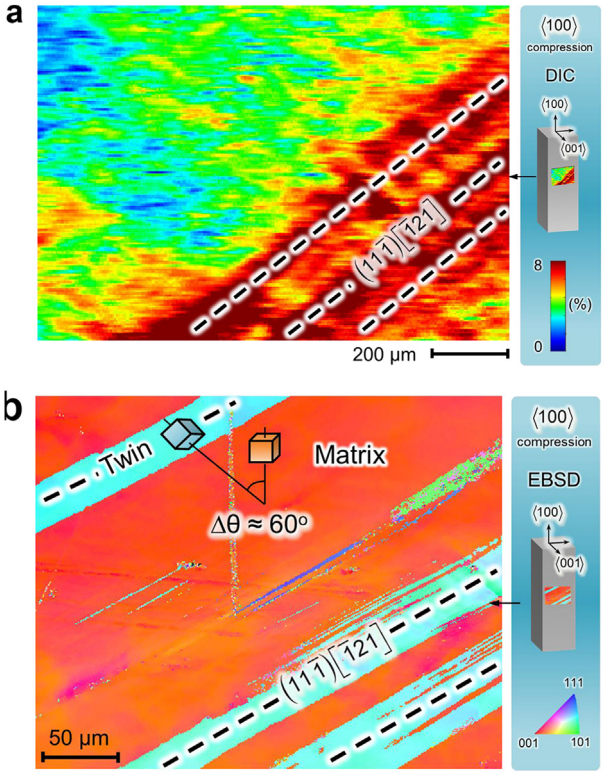

Fig. 9. (a) – In-situ DIC strain contour on the {001} surface is presented at a global strain level of 6% (⟨100⟩ compression). (b) – EBSD data on the {001} surface of the deformed specimen confirm the existence of a 60° (approximately) misorientation between the matrix and the strain band as illustrated with the rotated cubes (⟨100⟩ compression).

$$f(x-d) = b + \frac{b}{\pi}\left[\tan^{-1}\left(\frac{x}{\zeta}\right) + \tan^{-1}\left(\frac{x-d}{\zeta}\right)\right] \tag{2}$$

Where, x indicates any position on the slip plane along slip direction measured from the dislocation core; $b = |\vec{b}| = a_{Co-Ni}/\sqrt{6}$ is the magnitude of the partial dislocation's Burgers vector; ζ the core half-width of the individual partial ($\zeta_{screw} = a_{Co-Ni}/2\sqrt{3}$ and $\zeta_{edge} = a_{Co-Ni}/2\sqrt{3}(1-\upsilon)$; υ is Poisson's ratio, $\upsilon = -s_{12}/s_{11}$ (Ballato, 1996) (where, compliance elements s_{11} and s_{12} are determined from the stiffness constants, C_{11}, C_{12} and C_{44}, which are 238.7, 155.3 and 131.5 GPa, respectively (Weston and Granato, 1975)). By representing GSFE as a function of the disregistry function, $f(x-d)$ from Equation (2), one can express the total energy requirement, E_{GSFE} to create dislocation slip in a pristine crystal as in Equation (3) (Hirth and Lothe, 1982; Joos et al., 1994; Schoeck, 1994).

$$E_{GSFE} = \sum_{x=-\infty}^{x=+\infty} \gamma[f(x-d)]a' \tag{3}$$

Where, a' is the lattice periodicity i.e. shortest distance between two equivalent atomic rows in the Burgers vector direction ($a' = 2b = 2a_{Co-Ni}/\sqrt{6}$). In other words, the parameter a' is the total span of the GSFE curve (i.e. between two the fault energy values equal to zero). The quantity E_{GSFE} is computed numerically by fitting Frenkel type trigonometric expressions by disintegrating the total span of the GSFE (i.e. $a' = 2b$) into symmetric segments as in Equation (4). For the ease of numerical procedure, x can be written in terms of dislocation position, u as $x = ma' - u$; where, m is an integer ranging from $-\infty$ to $+\infty$. Since the range of GSFE or misfit energy is very short, the consideration of the infinite magnitude of m can be restricted to a large number instead during the calculation (i.e. ensuring the entire span of the GSFE i.e. for $a' = 2b$).

$$E_{GSFE} = \underbrace{2\sum_{m=-\infty}^{m=+\infty}\left[\gamma_{us} sin\frac{\pi f}{b}\right]\frac{b}{2}}_{\text{GSFE for } 0 \le u/b \le 0.5} + \underbrace{2\sum_{m=-\infty}^{m=+\infty}\left[\frac{\gamma_{us}+\gamma_{isf}}{2} - \frac{\gamma_{us}-\gamma_{isf}}{2} sin\frac{\pi f}{b}\right]\frac{b}{2}}_{\text{GSFE for } 0.5 < u/b \le 1} \tag{4}$$

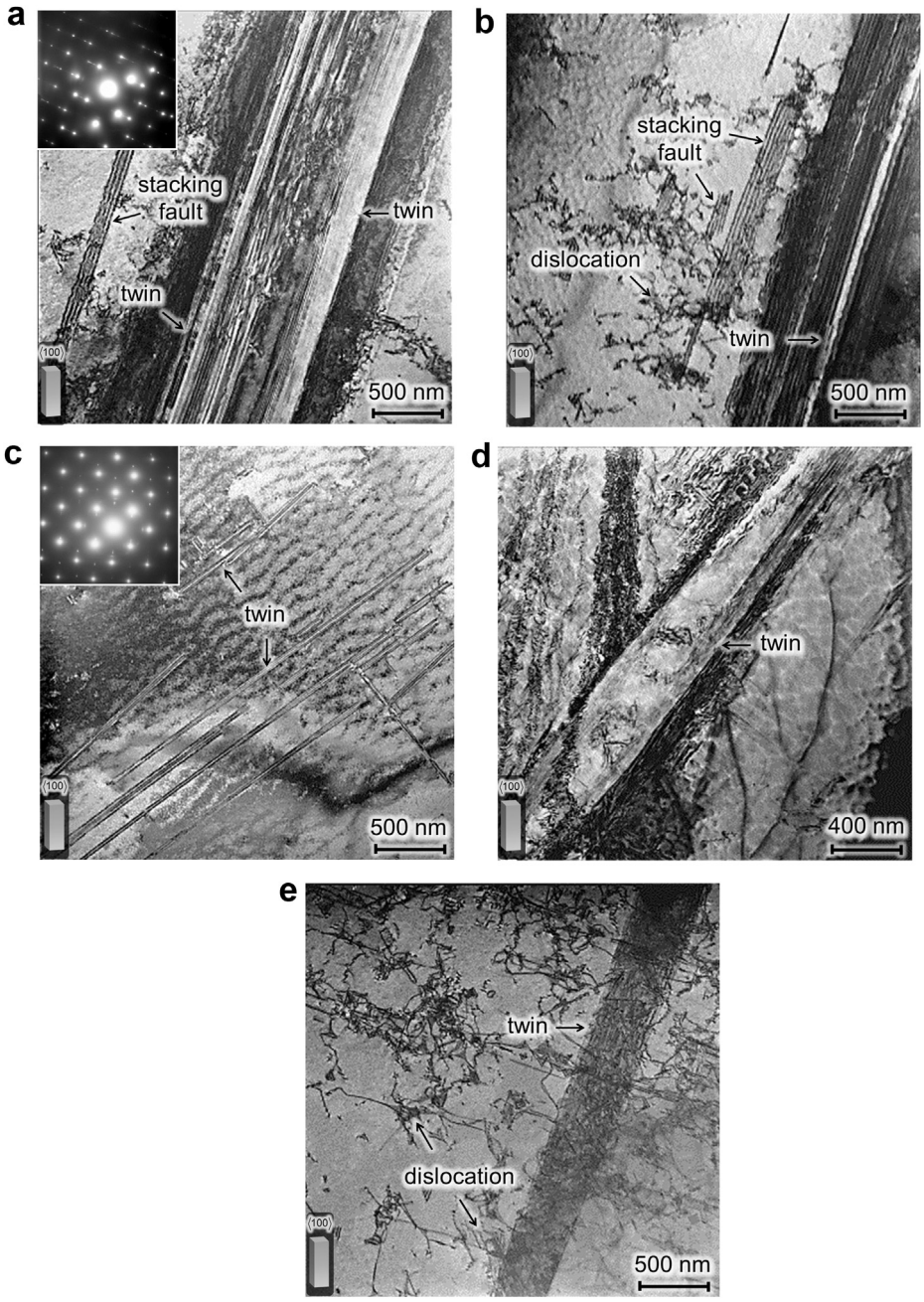

Fig. 10. (a) – Note the presence of mechanical twins along with stacking faults also supported by twin diffraction spots in the inset SAD pattern (⟨100⟩ compression). (b) – Evidence of twins, stacking faults and grouped dislocations (⟨100⟩ compression). (c) – Presence of fine twins can be seen as supported by the corresponding SAD patterns (⟨100⟩ compression). (d) – Note an advancing though grouped dislocations (⟨100⟩ compression). (e) – Further evidence of twin propagation through dislocation forest is clearly visible (⟨100⟩ compression).

The E_{GSFE} is evaluated numerically from Equation (4). The combined treatment of the GSFE and dislocation disregistry allows for predicting the theoretical critical resolved shear stress for slip nucleation (the Peierls stress), τ_{CRSS}^{slip} from Equation (5) (Hirth and Lothe, 1982; Joos et al., 1994; Schoeck, 1994).

$$\tau_{CRSS}^{slip} = \left(\frac{1}{b}\frac{dE_{GSFE}}{du}\right)_{max} \tag{5}$$

The thus-computed τ_{CRSS}^{slip} for Co-33%Ni alloy has been found to be 14 MPa. This value conforms to the experimentally determined τ_{CRSS} magnitude for the single crystals under ⟨123⟩ tension (15 ± 1.5 MPa), ⟨111⟩ compression (16 ± 1.2 MPa) and

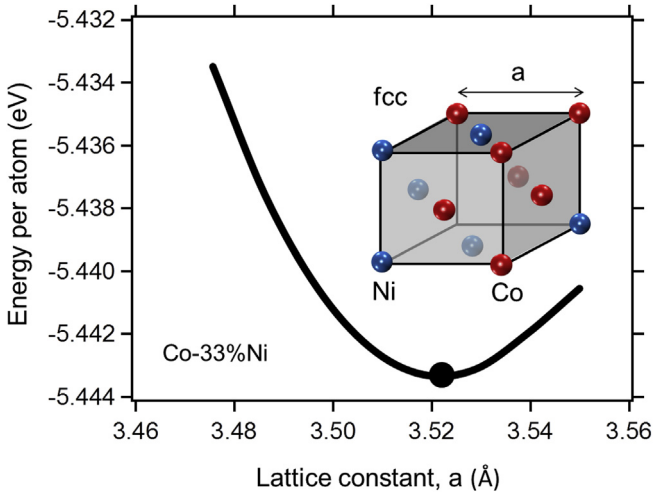

Fig. 11. The curve showing the per-atomic potential energy versus various levels of the lattice constant, $a_{Co\text{-}Ni}$, of the Co-33%Ni calculated from density functional theory (DFT). The magnitude of $a_{Co\text{-}Ni}$ corresponding to the minimum per-atom energy is considered the stable one (as highlighted with a solid circle).

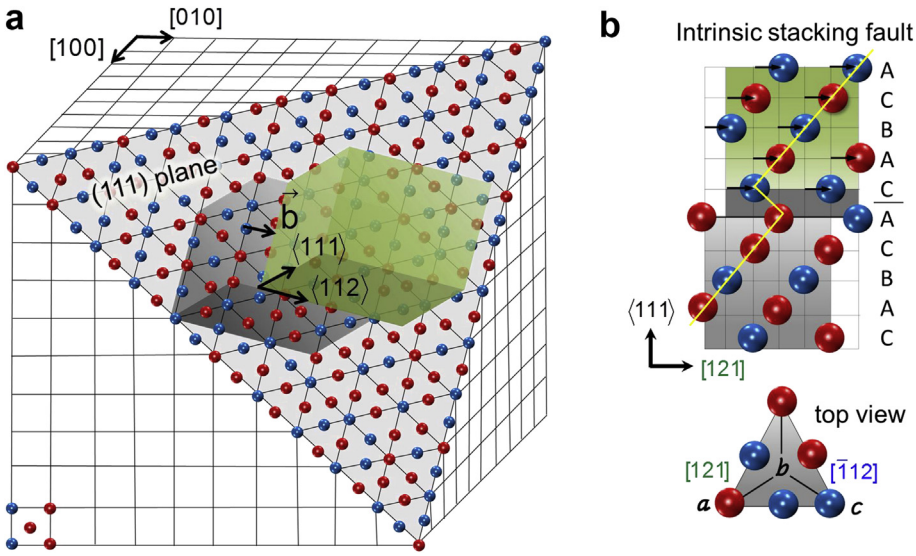

Fig. 12. (a) – A planar cutaway view of the close-packed (111) slip plane in the Co-33%Ni fcc lattice. Two crystal blocks with adjoining interface on the (111) slip planes (in green and gray) were rigidly displaced along the [121] direction in the DFT simulations to compute GSFE/GPFE landscapes. (b) – An example of the resultant structure from shearing of the two blocks in Fig. 12(a) by a displacement of $|\vec{b}|$ along the vector, $\vec{u}_{ab} = \vec{b} = a_{Co-Ni}/6[112]$. (For interpretation of the references to color in this figure legend, the reader is referred to the web version of this article.)

polycrystalline material in tension (16 ± 1 MPa). The comparison is summarized in Fig. 19. As elaborated in Section 3.2, these loading orientations have been found to be particularly conducive to slip nucleation. The reported error levels in the experimental values are attributed to the statistical average obtained from multiple experiments.

4.4. Generalized planar fault energy (GPFE)

Fig. 15 reports the DFT-calculated GPFE curve of the Co–33%Ni solid solution. As illustrated with the inset schematics, the perfect fcc lattice results in a stacking fault upon shearing along [121](a→b) by one Burgers vector. The associated γ energy profile corresponds to the first half portion of the GSFE curve from Fig. 13. However, the GPFE is generated via continued shear along the same crystallographic direction on consecutive parallel (111) planes. The adjoining atoms one layer above the stacking faults, upon displaced by 1b (resulting in a total displacement of 2b with respect to the initial perfect fcc configuration) creates a two-layer fault. The corresponding energy barrier i.e. the unstable twin fault energy, γ_{ut}, is found to be 216 mJ/m^2, and the coherent twin boundary energy, γ_{tsf}, is 10 mJ/m^2 (which is equal to $\gamma_{isf}/_2$). Translation by another Burgers vector on the adjacent atomic layer above the two-layer fault (i.e. 3b total displacement) generates a twin nucleus. Further

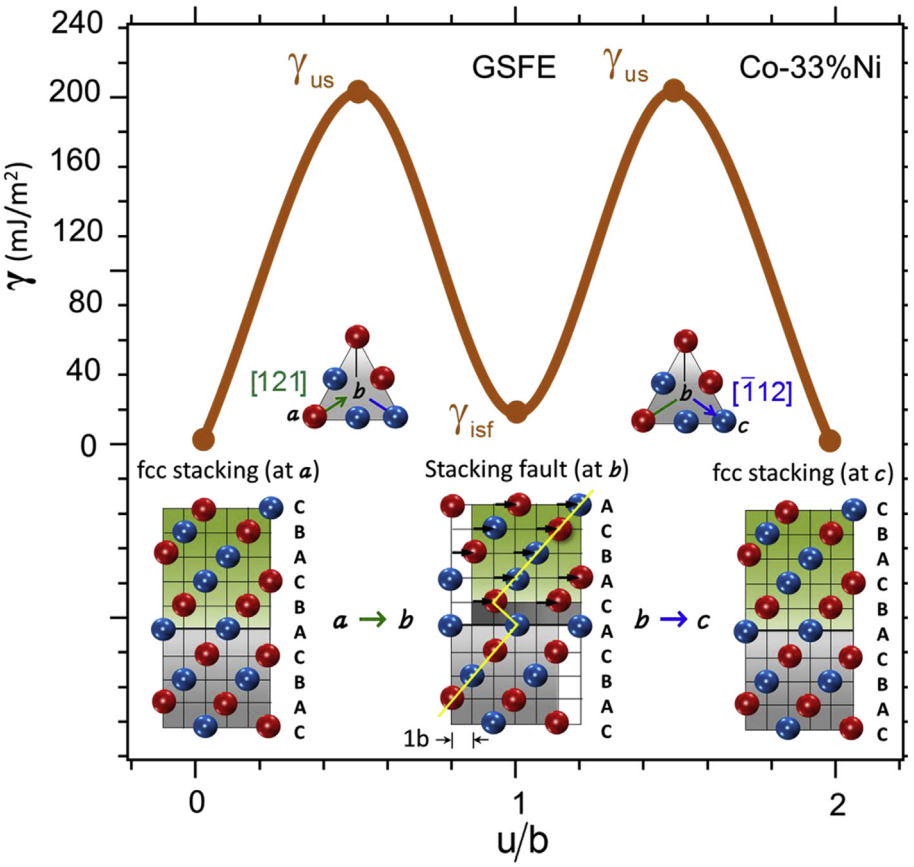

Fig. 13. DFT-computed generalized stacking fault energy (GSFE) profile of the Co-33%Ni solid solution.

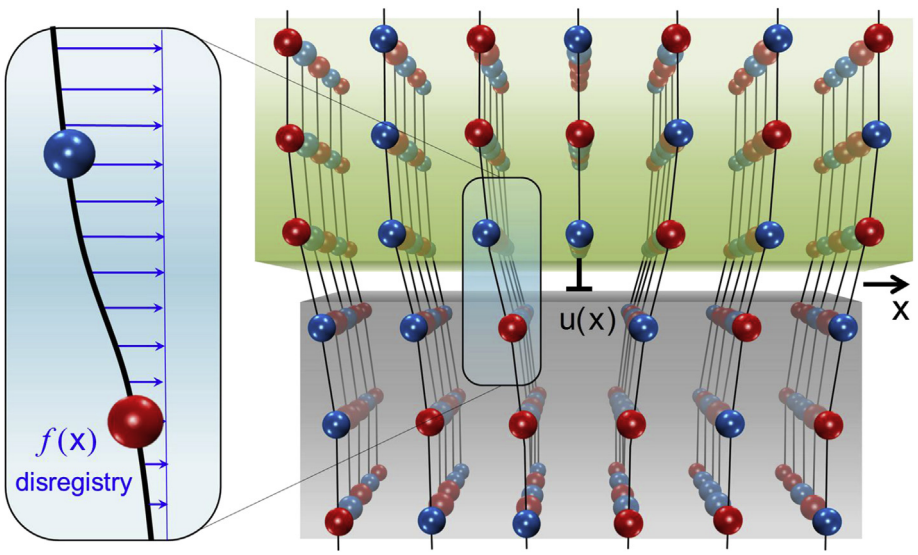

Fig. 14. The physical significance of the disregistry function, f(x) for the case of a full dislocation. The function f(x) captures the horizontal displacement differential of the atoms (before and after the occurrence of slip) across the glide plane at a distance, x, from the dislocation core.

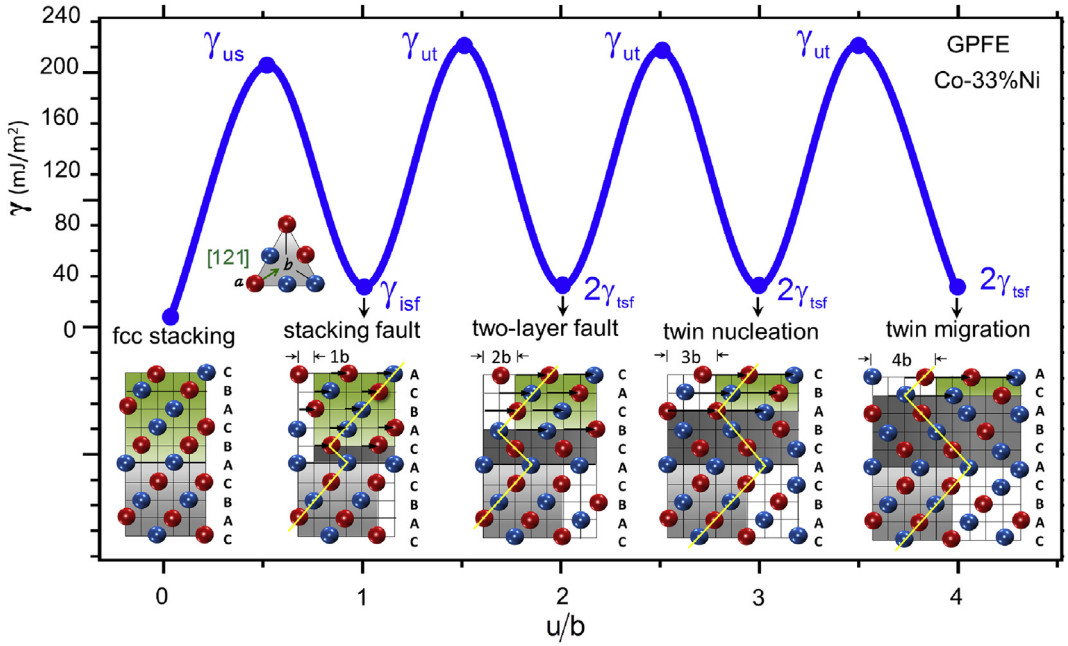

Fig. 15. DFT-calculated generalized planar fault energy (GPFE) curve of the Co-33%Ni solid solution. It represents the twin energy pathway.

displacement on successive layers above the twin nucleus culminates in the onset of the twin migration process, i.e. a layer-by-layer growth of the twin. In the following sections, we demonstrate that the consideration of the twinning energy pathway (i.e. the GPFE) is crucial in predicting the critical resolved shear stress for twin nucleation, τ_{CRSS}^{twin} as well as twin-slip interaction, $\tau_{CRSS}^{twin-slip}$.

4.5. Critical resolved shear stress for twin nucleation τ_{CRSS}^{twin}

Deformation twinning induces the shearing of discrete lattice at the atomic level. The GPFE landscape delineates the corresponding atomistic energy aspect. The physical process of mechanical twin nucleation is associated with successive

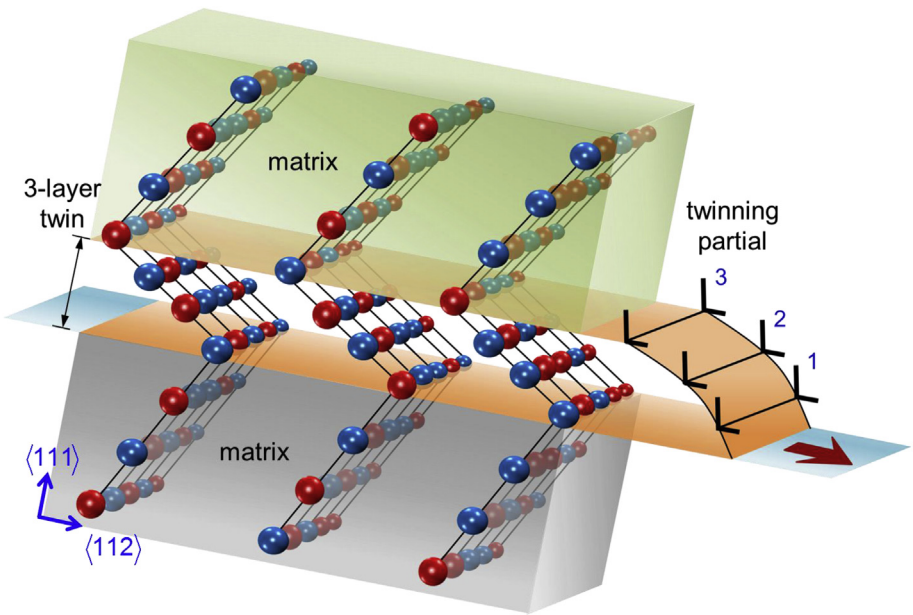

Fig. 16. The mechanism of twin nucleation via atomistic shearing of the crystal due to the sequential gliding of twinning partials on three parallel (111) planes.

passages of Shockley partial dislocations on consecutive glide planes (Blewitt et al., 1957; Venables, 1964a). Fig. 16 illustrates the mechanism of atomistic shearing of the crystal due to the sequential gliding of twinning partials of three parallel (111) planes. It is, therefore, imperative that, in addition to the atomic level energetics, the mutual elastic interaction and long-range disregistry effects of these twinning dislocations be considered to accurately predict the critical resolved shear stress for twin nucleation, τ_{CRSS}^{twin}. The applied shear stress to nucleate a twin ought to work against the elastic interaction effects as well as the periodic lattice resistance to atomic shear displacements. In the current model, we balance the total applied work with the energy expenditure to be overcome (i.e. total elastic interaction energy and shear-induced GPFE contributions) as follows in Equation (6).

$$\underbrace{tw\varepsilon_{twin}\tau_{CRSS}^{twin}}_{\text{applied work}} = E_{interaction} + E_{GPFE-nucleation}$$
$$= \underbrace{\frac{\mu_{\{111\}}b_{twin}^2}{4\pi(1-\upsilon)}\left(\ln\frac{D}{d_{1-2}}+\ln\frac{D}{d_{2-3}}+\ln\frac{D}{d_{1-3}}\right)}_{\text{interaction}} + \underbrace{\sum_{x=-\infty}^{x=+\infty}\gamma[f_{twin}(x,d_{1-2},d_{2-3},d_{1-3})]3b}_{\text{GPFE for nucleation:}1\le u/b\le 3} \quad (6)$$

Where, the twin thickness $t = 3a_{Co-Ni}/\sqrt{3}$(corresponding to the height of three (111)-type atomic layers); the width of the twin $w \approx 10t$ upon minimization of the total energy with respect to w and t (which is consistent with the w/t ratio reported in earlier literature) (Kibey et al., 2007; Koning et al., 2002); the twinning-induced eigenstrain $\varepsilon_{twin} = 1/\sqrt{2}$; the magnitude of the twinning dislocation Burgers vector $\vec{b}_{twin} = a_{Co-Ni}/6\langle 112\rangle$; the dimension of the single crystal containing the twin $D \approx 2000$ microns; the shear modulus $\mu_{\{111\}} = \frac{3C_{44}(C_{11}-C_{12})}{4C_{44}+C_{11}+C_{12}}$, where,$C_{11}$, C_{12} and C_{44} are 238.7, 155.3 and 131.5 GPa, respectively (Weston and Granato, 1975); the spacings among the twinning dislocations $d_{1-3} = \frac{\mu b_{twin}^2}{2\pi\gamma_{isf}}$, $d_{2-3} = 0.732d_{1-3}$ and $d_{1-2} = d_{1-3} - d_{2-3}$ as derived upon balancing the acting elastic forces (Sleeswyk, 1963); and the total disregistry of the three-layered twin $f_{twin}(x,d_{1-2},d_{2-3},d_{1-3}) = f(x-d_{1-2}) + f(x-d_{2-3}) + f(x-d_{1-3})$ from Equation (2). The disregistry associated with the deformation twin is obtained by assuming linear superposition of the pair-wise disregistries of the twinning partials, as though they are on the same glide plane. We note that a singular twinning dislocation induces long range elastic distortion, and the thickness of the nucleus is rather small compared to the elastic range of the disregistry. Therefore, the refinement of twinning disregistry distribution over three adjoining atomic planes (separated by $a_{Co-Ni}/\sqrt{3}$) would not significantly differ from the current assumption. The line energy contribution of individual dislocations is found to be insignificant compared to the rest energy terms; hence, not considered in the above formulation. The energy quantity, $E_{GPFE\text{-}nucleation}$, in Equation (6) is computed numerically by fitting the GPFE curve from Fig. 15 with multiple-segmented trigonometric functions (of the form: $\left(\gamma_{max}\sin\frac{\pi f}{b}\right)$, where γ_{max} refers to the respective peak for each segment) in the same manner as in Equation (4).

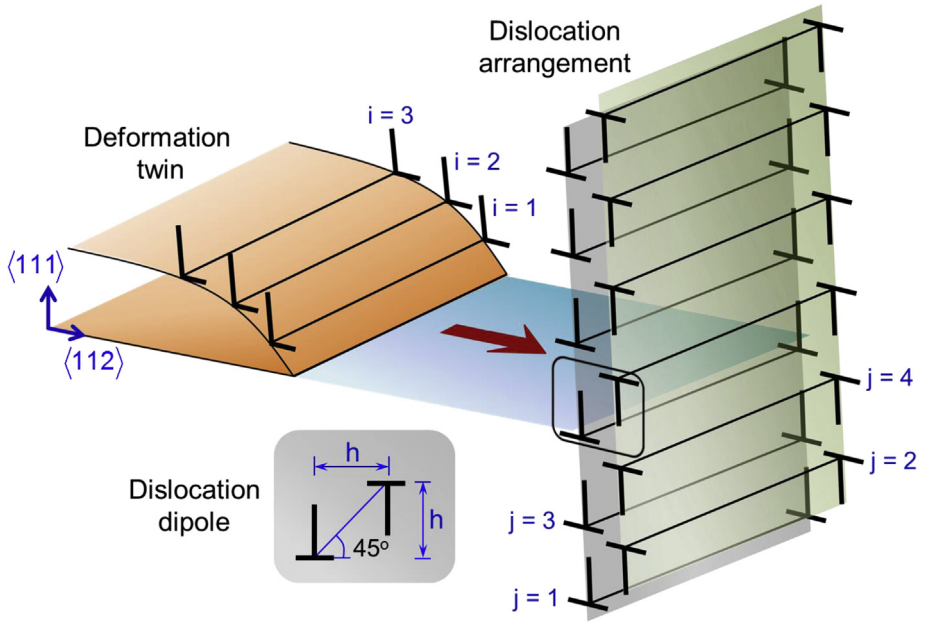

Fig. 17. A three-layer deformation twin (consisting of twinning partial dislocations) about to intercept a dislocation dipole arrangement.

From Equation (6), the theoretical critical twin nucleation stress, τ_{CRSS}^{twin}, has been determined to be about 26 MPa. This magnitude agrees well with the experimentally determined resolved yield stress (0.1% offset) for the single crystals oriented along ⟨111⟩ in tension (27 ± 5 MPa) and ⟨001⟩ in compression (26 ± 3 MPa). The comparison is presented in Fig. 19 It follows that the theoretical value is in good agreement with the experimental critical resolved shear stress for twinning. The reported error levels are due to the statistical average considered from a number of experiments.

4.6. Critical resolved shear stress for onset of twin–slip interaction $\tau_{CRSS}^{twin-slip}$

In order to model the critical shear stress for the onset of twin-slip interaction, we suppose an approaching three-layer deformation twin (consisting of twinning partial dislocations) about to intercept a dislocation arrangement as shown schematically in Fig. 17. We address this problem on the basis of classical continuum theory of applied work overcoming dislocation interaction energy complemented with the additional contribution from the GPFE considerations.

Fig. 17 illustrates the arrangement of the twin-slip interaction to be modeled. The twinning partials are designated with i = 1, 2 and 3. The obstacle dislocations are arranged in a columnar Taylor lattice configuration i.e. dislocation dipoles (i.e. a pair of dislocations of opposite signs placed at 45° with a spacing of h) aligned vertically. The effect of increasing h magnitudes (i.e. the horizontal and vertical dipole spacing) has been determined to reach a saturation level with respect to the model output; therefore, we assume the corresponding magnitudes of h (on the order of tens of Burgers vectors) for the current calculations. In the following equations, we designate the vertical dipole arrangement as the "wall". The vertical dislocations are labeled as j = 1, 2, 3, … N_{dipole} (odd numbers denoting the dislocations of one sign and the even the opposite). The consideration of a dipole array is rationalized due to the energetically stable configuration as reported earlier in the literature (Neumann, 1986). Nevertheless, other array configurations (e.g. non-dipole vertical arrangement) do not invoke significant deviation from the current prediction levels. The mechanics of the twin-slip interaction is described as follows.

In order for the oncoming twin to intercept the dislocation wall, the applied work ($W_{applied}$) ought to equal/surpass the combination of the total energy expense due to the interaction among the wall and the twinning dislocations (designated as $E_{twin-wall\ interaction}$) and the discrete lattice energy to be overcome ($E_{GPFE-migration}$). The $E_{twin-wall\ interaction}$ originates from the attractive or repulsive forces depending on the sign of the dislocation within each dipole (Hirth and Lothe, 1982). The $E_{GPFE-migration}$ is equivalent to the total energy related to the one-layer migration portion of the GPFE curve. The work-energy balance can be written as follows in Equation (7).

$$W_{applied} = E_{twin-wall\ interaction} + E_{GPFE-migration} \tag{7}$$

The term $W_{applied}$ for a twin of thickness t, situated at a distance d from the dislocation wall with a required shear stress of $\tau_{CRSS}^{twin-slip}$ is straightforward to establish as in Equation (8).

$$W_{applied} = t\, d\varepsilon_{twin} \tau_{CRSS}^{twin-slip} \tag{8}$$

For the term $E_{twin-wall\ interaction}$, let us consider the most simple hypothetical case of one twinning dislocation (with the Burgers vector magnitude b_{twin}) and one wall dislocation (b_{wall}), the elastic interaction among whose is given by the classical expression of $\frac{\mu b_{twin} b_{wall}}{4\pi(1-\upsilon)}\left(\ln\frac{D}{d}\right)$(where, D is the single crystal size) (Hirth and Lothe, 1982). Now, for an approaching twin nucleus (with three twinning dislocations i.e. $N_{twin} = 3$) and a dislocation wall with a number of (N_{wall}) dislocations, one has to consider the summation of individual twin-wall pair interactions. Now, since the assumed wall consists of dislocation dipoles, the wall dislocation of the same sign as the twinning dislocation will repulse, and that of the opposite sign will attract the twinning partials. Hence, there will be attraction/repulsion energy contribution. Considering all the foregoing factors, the total interaction energy between the oncoming twin and the dislocation wall, $E_{twin-wall\ interaction}$ can be written as follows in Equation (9).

$$E_{twin-wall\ interaction} = \underbrace{\frac{\mu b_{twin} b_{wall}}{4\pi(1-\upsilon)} \sum_{i=1}^{N_{twin}} \sum_{j=1}^{N_{wall}} (-1)^j \left(\ln\frac{D}{d_{i-j}}\right)}_{\text{elastic interaction}} \tag{9}$$

Where, d_{i-j} is the distance between the i-th twinning dislocation and j-th wall dislocation (which incorporates the horizontal/vertical dipole spacing, h).

Now, for the energy expense originating from shearing the discrete lattice during the twin-slip interaction, we consider the portion of the GPFE curve within the range $3 < u/b \leq 4$ as given in Equation (10).

$$E_{GPFE-migration} = \underbrace{\sum_{x=-\infty}^{x=+\infty} \gamma[f_{twin}(x, d_{1-2}, d_{2-3}, d_{1-3})]b}_{\text{GPFE for migration: } 3 < u/b \leq 4} \tag{10}$$

Hence, combining Equations (8)–(10), we obtain the Equation (11) where from the critical resolved shear stress for the onset of twin-slip arrangement interaction stress, $\tau_{CRSS}^{twin-slip}$ can be evaluated.

$$\underbrace{td\varepsilon_{twin}\tau_{CRSS}^{twin-slip}}_{\text{applied work}} = \underbrace{\frac{\mu b_{twin} b_{wall}}{4\pi(1-\upsilon)}\sum_{i=1}^{N_{twin}}\sum_{j=1}^{N_{wall}}(-1)^{j}\left(\ln\frac{D}{d_{i-j}}\right)}_{\text{elastic interaction}} + \underbrace{\sum_{x=-\infty}^{x=+\infty}\gamma[f_{twin}(x, d_{1-2}, d_{2-3}, d_{1-3})]b}_{\text{GPFE for migration: } 3 < u/b \leq 4} \tag{11}$$

Following Equation (11), (when the impinging mechanical twin is very close to the dislocation arrangement i.e. d in the range of 1–4 nm), the maximum magnitude of $\tau_{CRSS}^{twin-slip}$ is determined to be 38 MPa. This value is compared with the corresponding experimental flow stress (39 ± 10 MPa as indicated with solid red circle) in Fig. 19. It is important to note that experimentally it is rather challenging to pinpoint the exact flow stress for the onset of the twin-slip interaction from the stress–strain plots alone. We have considered the inflection point on the stress-strain curve (i.e. an abrupt change of the slope) following the initial yield as indicative of the interaction. We establish the CRSS value from the combination of the shear stress-strain curves and the ex-situ TEM images at low deformation level. We have conducted a number of low strain tension/compression experiments with corresponding TEM images at various strain levels. Upon inspecting the TEM images for the low strain cases (<1%), we have established that the ⟨111⟩ tension and the ⟨001⟩ compression cases give rise to yielding by twinning and subsequent twin-slip interactions. We note the critical resolved shear stress levels for the onset of twin-slip interactions for each set of experiments for ⟨111⟩ tension and ⟨001⟩ compression. In this manner, we measure the CRSS levels for the twin-slip interactions from a range of experiments to be 39 ± 10 MPa. By studying the flow behavior from a number of experiments, the error level in the experimental $\tau_{CRSS}^{twin-slip}$ magnitudes is established as shown (solid red circles) in Fig. 19.

It is important to take into account the parametric sensitivity of the geometric considerations on the model output, $\tau_{CRSS}^{twin-slip}$. From an elasticity theory standpoint, one may select from several combinations of the dislocation geometries (i.e. edge/screw or full/partial) as well as the array alignment/orientation (i.e. perpendicular or angled to the approaching twinning direction). In the current model, the selection of the twinning dislocations as $a/6\langle 112\rangle$ type Shockley partials and the obstacle dislocation arrangement as a vertical array of (screw/edge) dislocation dipoles provides the most reasonable agreement with the experimental observations. We note that consideration of other combination of geometric consideration (e.g. non-dipole vertical array of edge/screw/partial dislocations) does not pose any fundamental modification to the proposed theory. The levels of theoretical $\tau_{CRSS}^{twin-slip}$ obtained using various sets of geometric input are well within the range of experimental $\tau_{CRSS}^{twin-slip}$ values as indicated by the error bars in Fig. 19. Hence, we adhere to reporting only one consistent level of theoretical $\tau_{CRSS}^{twin-slip}$ corresponding to a fixed set of input constants, thereby facilitating comparison with the statistically averaged (over a number of tests) experimental results.

4.7. Critical resolved shear stress for forest hardening τ_{CRSS}^{forest}

For the case of slip-mediated plasticity (in $\langle 123\rangle_{tension}$ and $\langle 111\rangle_{compression}$), dislocations upon nucleation continue to glide on one slip system until the applied stress is sufficiently large to initiate secondary non-parallel systems. With increase in deformation, dislocations from either system cut through the other, giving rise to the initiation of the so-called forest hardening effects. That is to say, in order for the forest hardening to start influencing the global stress-strain response, a considerable extent of forest dislocation density is required. One may argue that the critical stress level for slip–slip interaction could be modeled as a problem of elastic dislocation interactions following the same approach as the previous case of twin-slip interaction. However, unlike the twin-slip interaction case, the degree of forest hardening stress level would be

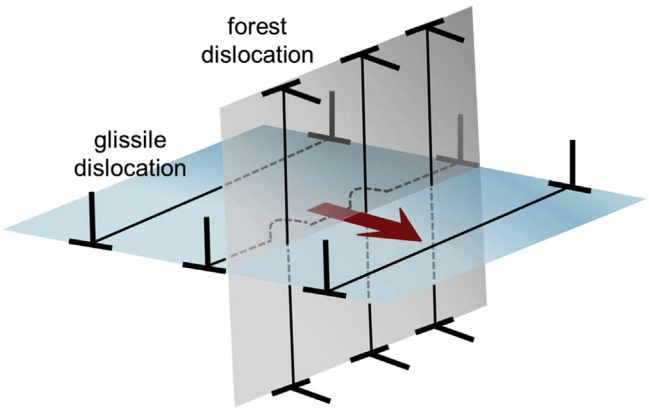

Fig. 18. The mechanism of forest hardening when a series of dislocations on one glide plane proceed to intercept dislocations on another slip system.

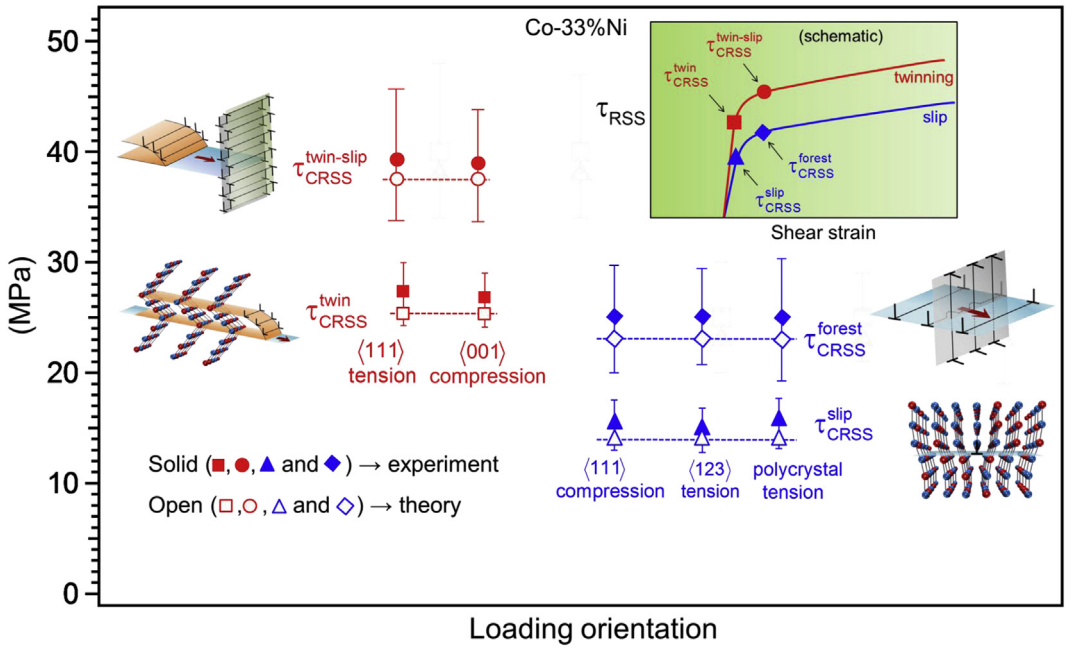

Fig. 19. Comparison of experimentally determined τ_{CRSS}^{slip}, τ_{CRSS}^{forest}, τ_{CRSS}^{twin} and $\tau_{CRSS}^{twin-slip}$ with the predicted values.

considerably affected by the mean dislocation spacing (as in Fig. 18) i.e. the dislocation density. Therefore, we deem it appropriate to resort to the classical treatment of the forest hardening as a direct function of the dislocation density (Estrin and Mecking, 1984) as given in Equation (12). Fig. 18 illustrates an example of glissile slip from one system cutting through (vertically arrayed) dislocations on another non-parallel slip system

$$\tau_{CRSS}^{forest} = \frac{\alpha\mu_{\{111\}}b}{\lambda} = \alpha'\mu_{\{111\}}b\sqrt{\rho} \tag{12}$$

Where, α and α' are constants specific to the material; ρ the dislocation density; λ the mean free path of gliding dislocations (considered along the dislocation motion direction).

We note that it is rather challenging to precisely establish the dislocation density from TEM study alone due to the limited portion of the material that the TEM images represent. Therefore, we adopt an ad hoc methodology on the basis of the current TEM analysis and the literature reported values of the dislocation density for the typical pre-deformation density. As pointed out earlier, we have conducted a number of experiments, and TEM images were taken at various global strain levels ex-situ. Upon inspecting the TEMs (which indicated massive slip–slip entanglement), we have pinpointed the initiation of the forest hardening following the nucleation of slip. Upon studying the slip morphology of the deformed microstructure for the slip-based hardening cases (i.e. for ⟨123⟩ tension and ⟨111⟩ compression) from the TEM analyses, we make an educated assumption of the dislocation density to be on the order of $10^{14}/m^2$ at the initiation of the forest interactions on an ad hoc basis.

Using Equation (12), the critical shear stress for the forest hardening initiation is determined to be about 24 MPa. The comparison with the experimental magnitudes (which is determined to be 25 ± 4 MPa from multiple experiments in ⟨123⟩ tension and ⟨111⟩ compression and polycrystalline tension) is provided in Fig. 19. We note the error level in the experimentally determined values, which arises owing to the difficulties in pinpointing the exact location on the stress-strain curve. We consider the sharp change of the strain–strain slope following the yielding to indicate the onset of the forest interaction mechanism (which is also supported by the TEM images taken at low global strain level).

5. Discussion

5.1. Flow behavior and microstructure evolution

In early literature, the plastic stress-strain behavior of fcc single crystals has been demarcated into three mechanistically distinct hardening regimes referred to as stage I, II and III (Friedel, 1955; Garstone and Honeycombe, 1957; Lomer, 1951). Upon yielding, the initial plasticity in the form of either slip or twin nucleation, precedes the more complex defect interplays of the ensuing hardening stages. Typically, stage I, II and III type strengthening behaviors originate from (i) easy dislocation glide restricted to few systems, (ii) multi-system poly-slip and (iii) dynamic recovery processes. The extent of all individual stages is reported to be a function of factors such as temperature, crystal purity, pre-existent dislocation density and crystallographic

orientation. Most recently, Kalidindi et al. (El-Danaf et al., 2001; Kalidindi, 1998) conducted extensive experimental and theoretical studies on characterizing the different hardening regimes of polycrystalline low SFE Co–Ni alloy deformed to large strain levels. The hardening stages of the present material Co-33%Ni are observed to be a strong function of the crystallographic orientation and the loading direction (Garstone and Honeycombe, 1957). In the current study, from the TEM studies of the post-deformation microstructure, the strain hardening of the Co-33%Ni single crystals in $\langle 123\rangle_{\text{tension}}$ and $\langle 111\rangle_{\text{compression}}$ occurs via extensive dislocation activities (with no twinning). From the stress-strain analysis, the initial $\langle 123\rangle_{\text{tension}}$ flow stress is found to be mostly non-hardening (i.e. having a low hardening coefficient $d\tau/d\gamma$) which complies with stage I type behavior. This observation is also consistent with the Schmid factor argument which, under $\langle 123\rangle_{\text{tension}}$ condition, predicts activation of only one slip system. The commencement of a distinct stage II hardening in this loading case occurs at higher strain levels (>10%). At this stage, the strengthening effects underlie glissile dislocations cutting through the pre-existent slip entanglements as revealed from the transmission electron micrographs. Classically, such a strengthening process is described by the so-called forest hardening (Basinski and Basinski, 1964; Estrin and Mecking, 1984) considerations, which dictate an empirical proportionality of flow stress to the square root of forest dislocation density. On the other hand, the material under $\langle 111\rangle_{\text{compression}}$ loading activates six slip systems in accordance with the Schmid law, immediately following the onset of yielding. The observed higher hardening rate in the $\langle 111\rangle_{\text{compression}}$ case can be attributed to extensive interactions among the multiple slip systems, conforming to the stage II type mechanism. In the early literature, Gerold and Karnthaler (Gerold and Karnthaler, 1989) reported the presence of wavy slip patterns in Co–Ni alloys. In the present study, we observe that the deformed microstructures under $\langle 123\rangle_{\text{tension}}$ and $\langle 111\rangle_{\text{compression}}$ demonstrate a considerable extent of stacking fault presence. Prevalence of stacking faults testifies to the existence of widespread dissociation of full dislocations into partials. In earlier experimental literature, the occurrence of partials is reported to be typical of low stacking fault energy materials. On the other hand, no evidence of deformation twinning is found for $\langle 123\rangle_{\text{tension}}$ and $\langle 111\rangle_{\text{compression}}$ although pervasive partial dislocation activities are known to be a prerequisite for twin nucleation.

Previous experimental literature (Christian and Mahajan, 1995; Paul et al., 2009; Skoczeń et al., 2010) reports fluctuating flow behavior in low stacking fault energy fcc metals and alloys. In the current investigation, Co-33%Ni under $\langle 111\rangle_{\text{tension}}$ and $\langle 100\rangle_{\text{compression}}$ exhibits somewhat serrated flow behavior, albeit with no significantly large drop. Based on the microstructural observation (via DIC, EBSD and TEM), the mechanistic origin of the flow fluctuation can be interpreted in terms of a dynamic process of twin nucleation and interaction with the existing dislocation arrangement. The macroscopic stress level undergoes a sudden attenuation as a consequence of accommodating local shear strains induced by twin nucleation. The follow-up stress upsurge occurs as the newly generated twin advances through sporadic pre-existent dislocation arrangements. Therefore, multiple nucleation events throughout the bulk of the material followed by interactions with slip cause the apparent raggedness to the flow curves under $\langle 111\rangle_{\text{tension}}$ and $\langle 100\rangle_{\text{compression}}$. It is worth noting that twinning induces a greater flow level than the slip based deformation. The present study (both theory and experiment) demonstrates a higher level of critical stress required to initiate twin-slip interactions (39 MPa) in Co–33%Ni, compared to mere twin nucleation (27 MPa) and slip nucleation (15 MPa) (values are approximate as indicated with error bars in Fig. 19). It is interesting to note that the critical shear stresses for twinning-related phenomena as well as slip are of similar orders of magnitude, unlike in typical fcc materials (where, critical twinning stresses are greater than slip by several orders of magnitudes). That is to say, it would suffice to consider only the Schmid law to rationalize the apparent orientation-dependence for the occurrence of the slip and twinning in the current material (Co-33%Ni alloy). On the basis of maximum Schmid factor argument, deformation twinning in Co-33%Ni alloy would occur only if the resolved shear stresses on the twinning systems exceed those on the slip systems (e.g. under $\langle 111\rangle_{\text{tension}}$ and $\langle 100\rangle_{\text{compression}}$), given the similarity of the corresponding critical stress levels.

It follows from the experimental stress-strain curves that twinning-dominated flow levels are considerably greater than the slip-induced plasticity. The TEM images have suggested that some extent of slip activities always accompany the observed twinning phenomena (especially, in the inter-twinning bands regions). Upon studying the behavior of polycrystalline Co-33% Ni Remy (Remy, 1978) attributed the twinning-induced augmented hardening effects to the obstruction of slip motion due to an abundance of newly-generated coherent twin boundaries. Remy argued that extensive twinning sub-divides a particular grain in multiple segments restricting the mobility of slip in the vicinity (either pre-existent or nucleated in concurrence with twinning), therefore, giving rise to Hall-Petch type strengthening effects. It is important to note that the current theory considers the case of an advancing twin front (modeled by a multi-layered arrangement of twinning partial dislocations), which approaches a dislocation array. The whole twin-slip intersection configuration has been treated as a problem of elastic interactions among continuum dislocations. In other words, the current model captures the elevated critical twin-slip interaction stress (as presented in Fig. 19) with fundamental elasticity theorems supplemented by atomic level shear contribution. One may argue that the problem could also be addressed via an analysis of dislocation slip impinging on migrating twin boundaries (resulting in elevated critical stress level). This type of investigation would essentially differ in details as reported in the earlier literature (Christian and Mahajan, 1995). The analysis of slip intercepting a twin boundary is compounded by different reaction outcomes, which are a strong function of local stress state and the nature of residual dislocations on the interface. There exists a considerable number of literature addressing the problem of slip intercepting a coherent twin boundary. We note that such an approach would essentially yield similar conclusions as from the current method i.e. the resultant elevation of the critical stress level, which is addressed by the authors in their earlier publications (Chowdhury et al., 2014a, b; Chowdhury et al., 2013). Therefore, the present treatment of twin-slip intersection based on basic elasticity assumptions is particularly advantageous, in that it provides a simple intuitive theory in good agreement with the experiments, circumventing the aforementioned complications (related with slip-intercepting-twin case).

Early literature notes that single crystals of conventional fcc metals undergo deformation twinning only at very high stress. For instance, pure Ni single crystals are reported to have twinning only preceding the ultimate fracture (Robertson, 1986). However, the present material, Co-33%Ni manifests a twinning stress level that is on the same order of magnitude with that of slip as observed experimentally. From the classical twinnability criterion (Miura et al., 1968; Pirouz, 1989; Venables, 1964b), the stacking fault energy (SFE or γ_{isf}) has been correlated as being proportional to the critical twinning stress (adjusted with some fitting constants). To illustrate this empirical trend, one may compare pure Ni (with a SFE of 127 mJ/m^2 (Beeston et al., 1968; Howie and Swann, 1961; Ogata et al., 2002)) with the current material Co-33%Ni (SFE being 20 mJ/m^2). Intuitively, the critical resolved shear stress for twinning in Co-33%Ni would be considerably lower (as currently determined to be about 27 MPa from Table 1) than that of pure Ni (predicted to be 250 MPa in earlier literature (Kibey et al., 2007)). However, It is quite intriguing to note that the critical resolved shear stress for slip in Co-33%Ni (about 16 MPa from current measurement from Table 1) is not significantly altered from that of pure Ni (about 9 MPa, from literature (Gottstein and Kocks, 1983; Mader et al., 1963)). This is an important observation that clearly demonstrates the insufficiency of the stacking fault energy, γ_{isf}, as the sole parameter to dictate both the slip and the twinning tendency simultaneously. While the classical SFE-based approach can qualitatively indicate the twinnability, it cannot provide a quantitative basis to compare the competition between slip and twinning. Moreover, the twinning-assisted flow is observed to demonstrate a superior hardening behavior compared to slip that apparently cannot be modeled solely based on the phenomenological parameter γ_{isf}. We address this dilemma by additionally incorporating the atomistic energy barriers γ_{us} (unstable stacking fault energy) and γ_{ut} (unstable twinning fault energy) into a Peierls-Nabarro based theory to quantify the critical slip/twin nucleation stresses.

Upon a careful review of the relevant literature, we note that the theoretical aspects of slip and twinning are not mutually exclusive. That is to say, the physical process of twin nucleation can be disintegrated into a problem of collective behaviors of twinning dislocations. Therefore, we consider a uniform Peierls-Nabarro modeling framework accompanied by necessary atomistic ingredients to rationalize the aforementioned quandary.

5.2. Prediction of slip, twin, twin–slip interaction

Theoretical quantification of slip nucleation stress in a pristine crystal has been treated universally by the Peierls-Nabarro model (Hirth and Lothe, 1982; Joos et al., 1994; Lu et al., 2000; Nabarro, 1947; Peierls, 1940; Schoeck, 1994). The basic premise thereof states that a dislocation in a metallic crystal is assumed to be embedded in a continuous elastic medium except for the slip plane (whereupon non-continuum discreteness is imposed). The continuum assumption of the metallic matrix serves to provide the solution of the disregistry function, f(x), owing to the elastic distortion of the crystal as in Equation (2) (illustrated in Fig. 14). The atomistic discreteness of the lattice is assumedly smeared upon the glide plane in the form of periodic energy topography. The early models (Hirth and Lothe, 1982; Nabarro, 1947; Peierls, 1940) considered sinusoidal energy profile on an ad hoc basis until recent advances (Lu, 2005; Schoeck, 2005) establish the generalized stacking fault energy (GSFE) profile as the most appropriate energetic representation of the lattice periodicity. As per the original Peierls-Nabarro proposition, the required critical stress to create dislocation slip amounts to the applied shear stress level to move the dislocation core and disregistry assembly through the periodic energy-displacement landscape. Therefore, it is imperative that both the elastic effects and the atomistic fault energy profile be considered simultaneously in quantifying the Peierls stress. In the current undertaking, we achieve that objective by numerically reconstructing the atomistically-computed GSFE as a function of the disregistry, f(x), in the form of a Fourier-type trigonometric series (as in Equation (4)). Given the complexity of the mathematical expression, it is deemed necessary to seek a numerical solution for the Peierls stress (from Equation (5)), rather than establishing a closed form analytical expression. The present numerical scheme is particularly advantageous, in that it does not incur an exponential dependence of the Peierls stress on the dislocation core width as reported in earlier literature (Joos et al., 1994). The reasonable agreement with the theoretical Peierls stress and the experimentally determined critical resolved shear stress (presented in Fig. 19) attests to the accuracy of the current method. Furthermore, we proceed to prove that the Peierls-Nabarro foundation can also be effectively utilized in modeling the critical twin nucleation stress.

Venables (1964b) first hypothesized the critical stress to nucleate a mechanical twin on the basis of overcoming the frictional resistance to create a plane with an intrinsic stacking fault. Subsequently, Pirouz (1989) improved the original Venables' assumption by incorporating the mobility differential between a leading and a trailing partial dislocation that tether the stacking fault end-to-end. Moreover, Miurat al. (1968) considered the formation of an extrinsic stacking fault (i.e. a two-layer fault) as a precursor to the twin nucleation. Karaman et al. (2000) extended this idea to incorporate solute drag effects. Meyers et al. (2001) conducted an Eshelby type analysis to incorporate deformation kinetics considerations (i.e. strain-rate, temperature etc.). All these theories are essentially phenomenological, in that they consider only the intrinsic stacking fault energy (SFE or γ_{isf}) as the material input parameter. From a thermodynamic perspective, Fischer et al. (Fischer et al., 2003) approached the problem by balancing the total interaction energy among a vertical arrangement of dislocations and mechanical work necessary to create a twinned region represented by its eigenstrain. Tadmor et al. (Tadmor and Bernstein, 2004; Tadmor and Hai, 2003) first proposed the necessity of assessing twinnability in fcc materials with a combined treatment of three fault energy parameters, i.e. γ_{isf}, γ_{us} (unstable stacking fault energy) and γ_{ut}(unstable twin fault energy) from first principles. They argued that it is equally vital to consider the unstable energies (γ_{us} and γ_{ut}), in conjunction with more traditionally used γ_{isf} to establish a comprehensive twinning criterion. However, it is important to note that prediction of the critical stress level, according to these models, is contingent upon the presence of a sufficiently high local stress concentration source (e.g. dislocation pile-up (Venables, 1964b), Lomer-Cottrell barrier (Karaman et al., 2000; Pirouz, 1989), grain boundary (Miura et al., 1968), dislocation wall (Fischer et al.,

Table 2
Summary of the experimentally extracted CRSS levels and the theoretical results (also, presented in Fig. 19).

Mechanism	Equations	Input parameters	Theoretical τ_{CRSS} (MPa)	Experimental τ_{CRSS} (MPa)
Slip nucleation	$\tau_{CRSS}^{slip} = \frac{1}{b}\left.\frac{\partial E_{GSFE}(\gamma_{isf},\gamma_{us})}{\partial u}\right\|_{max}$	$\gamma_{us} = 205 mJ/m^2$ $\gamma_{isf} = 20 mJ/m^2$ $b = a_{Co-Ni}/\sqrt{6}$ $a_{Co-Ni} = 3.521\ A^o$	14	15
Twin nucleation	$\tau_{CRSS}^{twin} = \frac{E_{interaction} + E_{GPFE-nucleation}(\gamma_{tsf},\gamma_{ut})}{tw\varepsilon_{twin}}$	$\gamma_{ut} = 216 mJ/m^2$ $\gamma_{tsf} = 10 mJ/m^2$ $t = 3a_{Co-Ni}/\sqrt{3}$ $w \approx 10t$ $\varepsilon_{twin} = 1/\sqrt{2}$	26	27
Onset of twin-slip interaction	$\tau_{CRSS}^{twin-slip} = \frac{E_{twin-wall\ interaction} + E_{GPFE-migration}(\gamma_{tsf},\gamma_{ut})}{td\varepsilon_{twin}}$	$\gamma_{ut} = 216 mJ/m^2$ $\gamma_{tsf} = 10 mJ/m^2$ $d \approx 3$ nm $\varepsilon_{twin} = 1/\sqrt{2}$	38	39
Onset of slip−slip interaction	$\tau_{CRSS}^{forest} = \alpha' \mu_{\{111\}} b\sqrt{\rho}$	$\alpha' = 0.2$ $\rho = 10^{14}/m^2$ $\mu_{\{111\}} = 35 GPa$	24	25

2003) or micro-crack (Tadmor and Bernstein, 2004) etc.) that can trigger the nucleation process. However, in a single crystal with the absence of the aforementioned sources, a deformation twin is more likely to nucleate near surface imperfection or bulk inhomogeneity. In such a case, it can be initiated from pre-existent dislocation conglomerates that are prone to dissociate into multi-layered stacking faults (Blewitt et al., 1957). In experimental literature, it is indicated through high resolution electron microscopy that some extent of slip activities precedes the mechanical twinning (Christian and Mahajan, 1995). It is now well-established that the mechanism of deformation twinning is analogous to a succession of Shockley partials on adjoining glide planes (as illustrated in Fig. 16). Consecutive shearing induced by each dislocation leads to the evolution of a twin nucleus via the creation of an intrinsic stacking fault followed by an extrinsic stacking fault. In the present work, we incorporate the combined disregistries of the participant twinning partials and the entire atomistic energy landscape, i.e. the GPFE, within a Peierls-Nabarro framework. This approach inherently allows for the inclusion of slip, intrinsic/extrinsic stacking fault generation as a precursor to the twin nucleation as classical theories dictate. As per the current experimental observation, the twin nucleus grows in thickness (also known as the twin migration) and advances to intercept a pre-existent dislocation arrangement. We model the critical stress to initiate twin-slip interaction by considering the underlying energy cost for the atomistic migration process as well as continuum interaction effects.

Elastic properties of dislocation walls (consisting of edge or screw type dislocations) and their interaction with approaching dislocations (edge or screw) have been discussed extensively by Li et al. (Li, 1960a, b; Li and Chalmers, 1963; Li and Needham, 1960). We approach the process of a twin intercepting a dislocation arrangement principally as a similar elastic problem with the addition of a migration-induced atomic shear contribution. The partial dislocations at the front of the advancing twin nucleus would experience attractive/repulsive forces from the dislocation wall arrangement. In the current model, we have considered a vertical dipole arrangement consisting of straight dislocations (as shown in Fig. 17). As suggested by Neumann (Neumann, 1986), a dipole wall will be energetically favorable upon minimizing the total elastic energy of the configuration under external shear stress. We note that a particular choice of wall anatomy (i.e. edge versus screw or full versus dissociated or single versus double column) does not alter the fundamental aspect of the current model, invoking only a slight sensitivity on the predicted critical stress levels (<8%). Moreover, given the effective range of the elastic influences, one can optimize the spacing between the impinging twin and the slip wall to rectify the predictions so as to reach an acceptably converged level. Thus, we adhere to the assumptions that produce the most reasonable agreement with the experimental critical resolved shear stress magnitudes (as compared in Fig. 19). A summary is provided in the form of Table 2.

The most important contribution of the current model can be deemed as establishing a theoretical framework to incorporate the GSFE and GPFE profiles into quantifying the aforementioned critical stresses. Thus, we essentially account for the underlying electronic effects of the alloy crystal to rationalize the slip and twinning phenomena both in a qualitative and quantitative manner.

5.3. Role of electronic structure and γ surfaces on deformation behavior

From the phase diagram of the Co–Ni alloy system, the current composition (67% Co) of the binary Co–Ni alloy possess a fcc crystal structure (Nishizawa and Ishida, 1983), while elemental Co and Ni are hcp and fcc crystals, respectively, at room temperature. It is well established in the earlier literature (Beeston et al., 1968; Gallagher, 1970; Howie and Swann, 1961) that the stacking fault energy, γ_{isf} of Co–Ni alloys gradually decreases with the addition of Co starting from the pure Ni level. The Co–Ni alloys possess neither long-range nor short-range ordering. These observations are consistent with the fact that both nickel and cobalt have similar physical, chemical and electronic properties. In particular, the near identical atomic volumes of elemental Ni and Co (Pfeiler, 2008) induce negligible elastic distortion upon mixing. Hence, the observed reduction in stacking fault energy from pure Ni level (127 mJ/m^2) to Co-33%Ni (20 mJ/m^2) can be elucidated in terms of the underlying solid state bonding effects.

Metallic bonding is characterized by a de-localized electron cloud shared by many atoms in the crystal lattice (Smallman and Bishop, 1999). From a quantum mechanical perspective, metallic deformation amounts to the collective translation of atomic nuclei embedded in such an electronic environment within the Born-Oppenheimer approximation (Tadmor and Miller, 2011). The electronic structure of the transition metals (Co and Ni) is especially dictated by their respective valence electron configuration. In particular, the state of complete or partial electron fulfillment of the d-orbitals critically influences the lattice bonding landscape, and hence governs the defect formation tendency. From a solid state physics standpoint, the origin of GSFE and GPFE profiles can be traced back to local variations in atomic bond strength as the gradual crystal shearing process creates various types of stable/unstable lattice structures (Ogata et al., 2002). That is to say, it is the electronic bonding strength among the nearest neighboring atoms in and around these faults that dictate γ surface levels in different metals and alloys. For instance, an intrinsic stacking fault in an otherwise perfect fcc lattice creates a local hcp structure. Thus, the apparent incongruity in the local atomic coordination would incur a considerable difference in bond lengths (and hence electron cloud density) among the fcc and hcp nearest neighbors surrounding the faulty lattice. The entire γ energy profile therefore quantifies the free energy differences to be overcome by external driving forces (e.g. applied stress) in order to nucleate a certain type of defect (e.g. intrinsic or extrinsic stacking faults, dislocation, twin boundary etc.). The so-called intrinsic stacking fault energy (SFE or γ_{isf}) in fact measures up to the differential of the hcp and fcc free energy density (per unit area). Intuitively, the free energy of a stacking fault in a solid solution would be a strong function of the solute atom concentration in the vicinity.

Early literature (Gallagher, 1970) reports that the gradual addition of Co to the pure nickel matrix reduces the SFE (from pure Ni level) to naught (corresponding to a composition demarcating the fcc-to-hcp transition, i.e. around 70% Co (Nishizawa and Ishida,

1983)). Suzuki (1962) observed that when the energy of the stacking fault in a crystal becomes negative, the fcc structure is no longer stable and hence tends to transform to a hcp lattice. In the current calculations, we observe that the abundance of Co also drastically reduces the γ_{us}(unstable stacking fault energy) and γ_{ut} (unstable twinning fault energy). Apostol and Mishin (Apostol and Mishin, 2011) demonstrated, in DFT simulations, that the distribution of the solute atoms relative to the fault substantially modifies the entire GSFE level. They revealed that if the solute atoms are located close to the fault, the corresponding fault energy reaches its minimum (which is known as the so-called Suzuki segregation). In the present quantum simulations, we distributed the solute atoms randomly throughout the base metal lattice on an iterative basis until the minimum energy configuration is obtained. Thus, we computed the minimum possible GSFE/GPFE levels that would be the most favorable energy pathway for the atomistic shearing of the material during slip/twinning. We emphasize that it is imperative to consider the entire GSFE and GPFE levels to glean a more complete comprehension of the observed slip characteristics and twinning propensity.

Van Swygenhoven et al. (2004) demonstrated the insufficiency of the classical approach of using the SFE as the only parameter to reconcile twinning and/or partial dislocation prevalence in a material. They proposed full consideration of the surface in the form of the ratio γ_{isf}/γ_{us} as the deciding parameter to justify the prevalence of full versus extended dislocations (especially when the material predominantly deforms by slip). They argued that a lowered γ_{isf}/γ_{us} ratio would indicate a greater propensity towards dissociation into partials (with increasing splitting distance between the partials). Separated partials are connected by a plane with a stacking fault with a fault energy density equal to the γ_{isf}. Upon the nucleation of the leading partial (by overcoming the energy barrier γ_{us}), the trailing partial ought to exceed a quantity equivalent to $(\gamma_{us}-\gamma_{isf})$. That is to say, a large difference between γ_{isf} and γ_{us} promotes splitting of full dislocations into partials. In the current TEM studies, a considerable amount of extended dislocation activities has been observed. Such a trend can be understood consulting the nature of the computed GSFE in terms of the γ_{isf}/γ_{us} level (which is computed to be 0.097 for Co-33%Ni). On the basis of a similar argument, experimentally equal propensity of twinning relative to the slip is also reflected in the GPFE landscape as the γ_{ut}/γ_{us} ratio tends to unity (calculated to be 1.0455) for Co-33%Ni. This result suggests that the current material uniquely possess nearly identical energy barriers for slip and twin nucleation. This is an important observation, in that experimentally only the Schmid factor has been found to dictate the initiation of either slip or twinning (indicating the existence of similar material resistance towards these two competing modes of plasticity).

5.4. Impact of current work and future challenges

The principal objective of the current undertaking is to address the inherent material preference for initiating plastic deformation by slip or twinning from the first principles. The present work provides quantitative evidence that the preferred plastic mechanism is governed by the quantum level fault energetics. The current emphasis is on predicting the critical stresses for initiating plastic flow via slip, twinning and twin-slip interactions. We chose to model the nucleation of slip and twinning at small strains (<1%). It is well established that the initiation of the macroscopic yielding (following the elastic deformation) is equivalent to overcoming the respective critical resolved shear stresses (CRSS) (for slip or twinning) at the microscale. However, the latter stage of plasticity involves multiple mechanisms contributing to the flow resistance at the mesoscale (sub-micron). On the other hand, the onset of plasticity is primarily governed by the atomistic lattice shear resistance (in the form of GSFE/GPFE energetics) originating at the sub-nanometer atomic lengthscale. At the elastic–plastic transition, the applied forces are spent in overcoming the lattice resistance for the slip/twin nucleation. Hence, it is rational to directly use the GSFE/GPFE levels to predict the mesoscopic critical resolved shear stresses (CRSS) within the Peierls-Nabarro framework. The reasonable agreement between the predicted and the experimental values of the CRSS lends sufficient credence to the current assumptions. The current research could be deemed as a step forward in understanding the inherent materials deformation propensity using ab initio techniques.

However, the deformation scenario becomes gradually more complicated for the post-yield stages as the extent of plasticity continues to evolve. For such a case, the mesoscopic deformation process would be characterized by extensive defect interactions, whose nature will play critical roles in the flow behavior. The current TEM, DIC and EBSD results serve to reveal the existence of competing deformation mechanisms (i.e. slip versus twinning) at higher strain levels (>6%) in the current Co–Ni alloys. As clarified earlier, the present work from a theoretical perspective) focuses on modeling the critical stresses to initiate plasticity, not the evolution thereof. However, the microstructure analyses via the optical techniques suggest the need of a comprehensive modeling framework for a complete understanding of the entire spectrum of stress-strain response. For example, the mesoscale plastic processes at large strains (at >6%) involves massive degrees of defect dynamics, the volume fraction evolution (of slipped and/or twinned regions) and the complex interlocking mechanisms (as observed by the TEM micrographs). The flow resistance at this stage is contributed by a number of deformation mechanisms. To that end, the Peierls-Nabarro formalism alone is insufficient, and cannot directly relate the atomistic GSFE/GPFE level with the continuum level flow behavior (without considering the extensive mesoscopic defect dynamics). The sub-nanometer quantum effects and the continuum mechanical behavior need to be bridged via extensive mesoscale defect modeling. Therefore, it is evident that not all processes can be fully covered at the present stage. As follows, we discuss the possible extension of the current model.

The current model can be extended by coupling the quantum contributions with: (a) the dislocation dynamics corresponding to large strain plasticity, and (b) the consideration of rate- and temperature-dependent flow behavior. To address the large deformation problem, the most significant extension of the current model can be conducted in the form of incorporating the dislocation dynamics simulations at the mesoscale (Amodeo and Ghoniem, 1990; Devincre et al., 2001). The slip

and twinning phenomena can be modeled separately through a statistically representative model of crystal plasticity (Cai and Bulatov, 2004). Through dislocation dynamics, the multiple contributions to the flow resistance at the larger strain regimes could be quantified from extensive defect interactions at the mesoscale (as also informed by the underlying quantum effects from the nanoscale, which the present work particularly brings into light for the initial plasticity). It would be of great interest to develop such a combined quantum mechanics-dislocation dynamics model, which would generate new knowledge on designing novel alloys with superior deformation properties.

For the present Co–Ni alloys, the Peierls-Nabarro based theory provides accurate predictions of the slip versus twinning CRSS levels independent of any temperature and strain-rate input. In the literature, there are evidences that the competition between the dislocation glide and the twinning in some low stacking fault fcc alloys can also be influenced thermally and/or by the deformation rate (Clayton, 2010b). In order to develop a generic model, the current theory could be incorporated with the principles of the deformation kinetics (Kocks et al., 1975). The rate/temperature-dependent flow mechanisms obey the Arrhenius type laws, which dictate an exponential dependence on an "energy barrier". In that regard, the current calculations provide evidence of the unstable stacking fault energy, γ_{us}, being the most deciding energy barrier parameter to quantify the resistance to plastic flow. These implications pave the way for the scientific community to further explore the materials microstructure-property correlation.

6. Conclusion

The current research documents the deformation behavior of single crystal Co-33%Ni alloy. The major contributions can be synopsized as follows:

1) Experimental monotonic strain hardening behaviors of the Co-33%Ni single crystals under tensile and compressive loading have been studied extensively. Two different modes of plasticity (slip and twinning) were observed as a function of crystallographic orientation and loading direction, triggered by the maximum Schmid factor on the respective systems. The crystals stressed in tension along ⟨111⟩ and ⟨100⟩ orientations undergo twinning, while compression induces extensive partial dislocation-mediated plasticity in ⟨123⟩ and ⟨111⟩-oriented samples. Twinning-induced plasticity demonstrates superior hardening behavior compared to that of dislocation slip. Critical resolved shear stresses corresponding to the initiation of twinning, twin-slip interaction, slip and forest hardening (slip–slip interaction) are measured from the experimental stress-strain curves as 27 MPa, 39 MPa, 15 MPa and 24 MPa respectively, also to be compared with theoretical predictions.
2) An assortment of experimental visualization techniques (DIC, EBSD and TEM) were employed to pinpoint the exact plastic flow mechanism in the individual loading cases. These methods assist in garnering an in-depth understanding of the macroscale flow behavior with the microscopic defect evolution mechanism (e.g. slip and twin nucleation, forest hardening, twin-slip interaction). These experimental observations unearthing the microscale defect dynamics help lay the foundation of a comprehensive theoretical framework to rationalize the observed trends in plasticity from an ab-initio perspective.
3) A physical theory is forwarded to account for the material predilection for slip and twinning in a both qualitative and quantitative manner. In particular, GSFE and GPFE landscapes were computed for a Co–33%Ni solid solution. A Peierls-Nabarro framework accompanied by requisite continuum considerations was employed to predict critical slip, twin and twin-slip interaction initiation stresses. A reasonable agreement of these theoretical stresses with the experimentally-determined CRSS levels attests to the validity of the modeling assumptions. The theoretical aspects of the current study in particular serve to incorporate the first principle based material parameter (e.g. γ_{us}, γ_{ut}) into the classical continuum context of slip and twinning.

7. Acknowledgment

This research was supported by the Nyquist chair funds and partially by NSF DMR-08-03270. The authors are grateful to Professor Yuri Chumlyakov at Siberian Physical Technical Institute, Russia for growing the Co–Ni single crystals. We acknowledge the use of the parallel computing resource, the Taub cluster, at the University of Illinois.

Appendix A. Polycrystalline experiments

Figure A1 reports the applied (global) stress-strain ($\sigma - \varepsilon$) curve for polycrystalline Co–33%Ni for small strain. The flow stress demonstrates raggedness to some extent. As no texture preference was found in the polycrystalline specimen, Taylor's assumption was used to extract the critical resolved shear stress (τ_{CRSS}) for plastic flow initiation using the following equation.

$$\tau_{CRSS} = \frac{\sigma_{yield}}{M} \tag{13}$$

Where, σ_{yield} is the macroscopic yield strength (0.1% offset) from the $\sigma - \varepsilon$ plot (48 ± 3 MPa) and M is the so-called Taylor factor (for isotropic fcc materials, M = 3.06). Using this method, τ_{CRSS} is measured to be 16 ± 1 MPa. This result is compared

with single crystal experimental data (from ⟨123⟩ tension and ⟨111⟩ compression) on τ_{CRSS} as well as the predicted value as compared in Fig. 19. It can be concluded from this comparison that the polycrystalline yield corresponds to dislocation slip nucleation. Subsequent flow proceeds in the form of forest dislocation hardening for which the critical stress level is determined to be 25 ± 6 MPa as listed in Fig. 19. We note that twinning in the polycrystalline sample is not evidenced for the initial stage of plasticity (as shown in the TEM images in Figure A2 and A3). However, the raggedness of the flow curve in Figure A1 indicates that twinning may occur at higher strain levels in favorably oriented grains (as the twinning Schmid factor exceeds that of dislocation slip in these grains). For the current modeling considerations, we limit our predictions to initial plasticity (corresponding to the material yield) and post-yield secondary plasticity (immediately following). Hence, latter stages of flow in the polycrystalline material (possibly contributed by twinning in addition to slip) are not investigated (experimentally or theoretically).

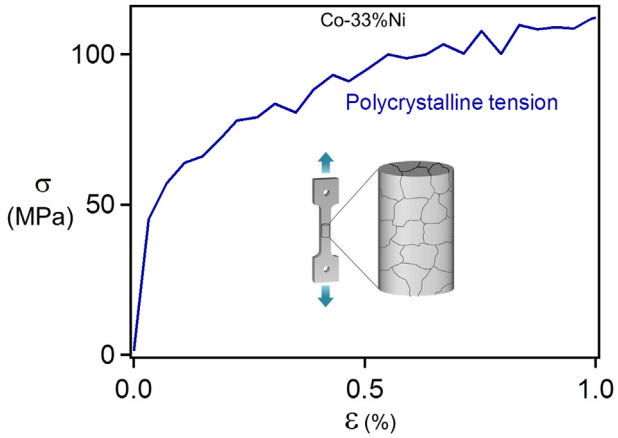

Fig. A1.

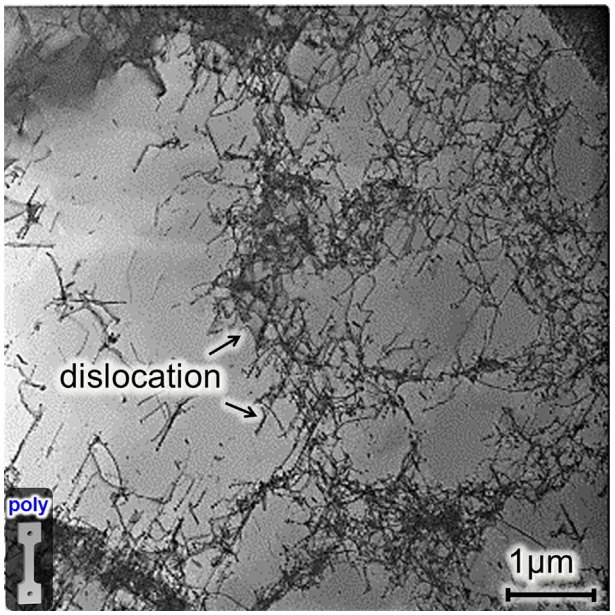

Fig. A2.

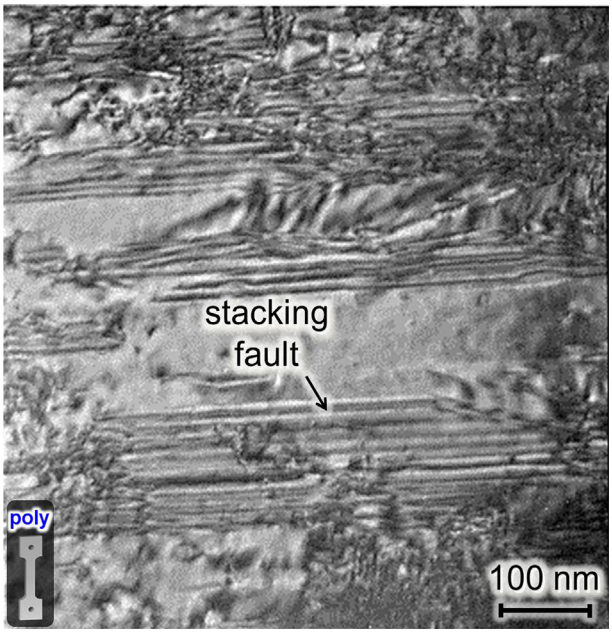

Fig. A3.

References

Amodeo, R., Ghoniem, N., 1990. Dislocation dynamics. I. A proposed methodology for deformation micromechanics. Phys. Rev. B 41, 6958.
Apostol, F., Mishin, Y., 2011. Hydrogen effect on shearing and cleavage of Al: a first-principles study. Phys. Rev. B 84, 104103.
Ballato, A., 1996. Poisson's ratio for tetragonal, hexagonal, and cubic crystals. IEEE Trans. Ultrasonics Ferroelectr. Freq. Control 56–62.
Basinski, Z., Basinski, S., 1964. Dislocation distributions in deformed copper single crystals. Philos. Mag. 9, 51–80.
Beeston, B., Dillamore, I., Smallman, R., 1968. The stacking-fault energy of some nickel-cobalt alloys. Metal Sci. 2, 12–14.
Blewitt, T., Coltman, R., Redman, J., 1957. Low-Temperature deformation of copper single crystals. J. Appl. Phys. 28, 651–660.
Cai, W., Bulatov, V.V., 2004. Mobility laws in dislocation dynamics simulations. Mater. Sci. Eng. A 387, 277–281.
Chowdhury, P.B., Sehitoglu, H., Rateick, R.G., 2014a. Predicting fatigue resistance of nano-twinned materials: part I–role of cyclic slip irreversibility and Peierls stress. Int. J. Fatigue 68, 277–291.
Chowdhury, P.B., Sehitoglu, H., Rateick, R.G., 2014b. Predicting fatigue resistance of nano-twinned materials: part II–effective threshold stress intensity factor range. Int. J. Fatigue 68, 292–301.
Chowdhury, P.B., Sehitoglu, H., Rateick, R.G., Maier, H.J., 2013. Modeling fatigue crack growth resistance of nanocrystalline alloys. Acta Mater. 61, 2531–2547.
Christian, J.W., Mahajan, S., 1995. Deformation twinning. Prog. Mater. Sci. 39, 1–157.
Clayton, J., 2010a. Modeling finite deformations in trigonal ceramic crystals with lattice defects. Int. J. Plasticity 26, 1357–1386.
Clayton, J., Knap, J., 2013. Phase-field analysis of fracture-induced twinning in single crystals. Acta Mater. 61, 5341–5353.
Clayton, J.D., 2010b. Nonlinear Mechanics of Crystals. Springer Science & Business Media.
Cooper, R., 1965. The equilibrium shape of deformation twins. Acta Metall. 13, 46–48.
Cottrell, A., 2000. An Introduction to Metallurgy. Universities Press.
Davis, J.R., 2000. Nickel, Cobalt, and Their Alloys. ASM international.
Devincre, B., Kubin, L., Lemarchand, C., Madec, R., 2001. Mesoscopic simulations of plastic deformation. Mater. Sci. Eng. A 309, 211–219.
Dreizler, R.M., Engel, E., 2011. Density Functional Theory. Springer.
Egner, H., Skoczeń, B., 2010. Ductile damage development in two-phase metallic materials applied at cryogenic temperatures. Int. J. Plasticity 26, 488–506.
El-Danaf, E., Kalidindi, S.R., Doherty, R.D., 2001. Influence of deformation path on the strain hardening behavior and microstructure evolution in low SFE FCC metals. Int. J. Plasticity 17, 1245–1265.
Estrin, Y., Mecking, H., 1984. A unified phenomenological description of work hardening and creep based on one-parameter models. Acta Metall. 32, 57–70.
Fischer, F., Appel, F., Clemens, H., 2003. A thermodynamical model for the nucleation of mechanical twins in TiAl. Acta mater. 51, 1249–1260.
Friedel, J., 1955. CXXX. On the linear work hardening mate of face-centred cubic single crystals. Philos. Mag. 46, 1169–1186.
Gallagher, P., 1970. The influence of alloying, temperature, and related effects on the stacking fault energy. Metall. Trans. 1, 2429–2461.
Garstone, J., Honeycombe, R., 1957. Dislocations and Mechanical Properties of Crystals. J. Wiley, New York, p. 391.
Gerold, V., Karnthaler, H., 1989. On the origin of planar slip in fcc alloys. Acta Metall. 37, 2177–2183.
Gottstein, G., Kocks, U., 1983. Dynamic recrystallization and dynamic recovery in< 111> single crystals of nickel and copper. Acta Metall. 31, 175–188.
Hirth, J.P., Lothe, J., 1982. Theory of Dislocations.
Hong, C., Tao, N., Lu, K., Huang, X., 2009. Grain orientation dependence of deformation twinning in pure Cu subjected to dynamic plastic deformation. Scr. Mater. 61, 289–292.
Howie, A., Swann, P., 1961. Direct measurements of stacking-fault energies from observations of dislocation nodes. Philos. Mag. 6, 1215–1226.
Humphrey, W., Dalke, A., Schulten, K., 1996. VMD: visual molecular dynamics. J. Mol. Graph. 14, 33–38.
Jin, Z., Bieler, T.R., 1995. An in-situ observation of mechanical twin nucleation and propagation in TiAl. Philos. Mag. A 71, 925–947.
Joos, B., Ren, Q., Duesbery, M., 1994. Peierls-Nabarro model of dislocations in silicon with generalized stacking-fault restoring forces. Phys. Rev. B 50, 5890.
Kalidindi, S.R., 1998. Modeling the strain hardening response of low SFE FCC alloys. Int. J. Plasticity 14, 1265–1277.
Karaman, I., Sehitoglu, H., Gall, K., Chumlyakov, Y., Maier, H., 2000. Deformation of single crystal Hadfield steel by twinning and slip. Acta mater. 48, 1345–1359.
Kibey, S., Liu, J., Johnson, D., Sehitoglu, H., 2007. Predicting twinning stress in fcc metals: linking twin-energy pathways to twin nucleation. Acta Mater. 55, 6843–6851.
Kocks, U.F., Argon, A.S., Ashby, M.F., 1975. Thermodynamics and kinetics of slip. Prog. Mater. Sci. 19.

Koning, M.d., Miller, R., Bulatov, V., Abraham, F.F., 2002. Modelling grain-boundary resistance in intergranular dislocation slip transmission. Philos. Mag. A 82, 2511–2527.
Kresse, G., Furthmüller, J., 1996. Efficiency of ab-initio total energy calculations for metals and semiconductors using a plane-wave basis set. Comput. Mater. Sci. 6, 15–50.
Kresse, G., Hafner, J., 1993. Ab initio molecular dynamics for open-shell transition metals. Phys. Rev. B 48, 13115.
Li, J., 1960a. The interaction of parallel edge dislocations with a simple tilt dislocation wall. Acta Metall. 8, 296–311.
Li, J., 1960b. Some elastic properties of an edge dislocation wall. Acta Metall. 8, 563–574.
Li, J., Chalmers, B., 1963. Energy of a wall of extended dislocations. Acta Metall. 11, 243–249.
Li, J.C., Needham, C.D., 1960. Some elastic properties of a screw dislocation wall. J. Appl. Phys. 31, 1318–1330.
Liu, Y., Bufford, D., Rios, S., Wang, H., Chen, J., Zhang, J., Zhang, X., 2012. A formation mechanism for ultra-thin nanotwins in highly textured Cu/Ni multilayers. J. Appl. Phys. 111, 073526.
Liu, Y., Jian, J., Chen, Y., Wang, H., Zhang, X., 2014. Plasticity and ultra-low stress induced twin boundary migration in nanotwinned Cu by in situ nanoindentation studies. Appl. Phys. Lett. 104, 231910.
Lomer, W., 1951. A dislocation reaction in the face-centred cubic lattice. Philos. Mag. Ser. 7 (42), 1327–1331.
Lu, G., 2005. The Peierls—Nabarro Model of Dislocations: a Venerable Theory and its Current Development. In: Handbook of Materials Modeling. Springer, pp. 793–811.
Lu, G., Kioussis, N., Bulatov, V.V., Kaxiras, E., 2000. The peierls-nabarro model revisited. Philos. Mag. Lett. 80, 675–682.
M'Guil, S., Wen, W., Ahzi, S., Gracio, J.J., Davies, R.W., 2014. Analysis of shear deformation by slip and twinning in low and High/medium stacking fault energy fcc metals using the ϕ -Model. Int. J. Plasticity 68, 132–149.
Mader, S., Seeger, A., Leitz, C., 1963. Work hardening and dislocation arrangement of FCC single crystals. I. Plastic deformation and slip line studies of nickel single crystals. J. Appl. Phys. 34, 3368–3375.
McDowell, D.L., 2010. A perspective on trends in multiscale plasticity. Int. J. Plasticity 26, 1280–1309.
Meyers, M., Vöhringer, O., Lubarda, V., 2001. The onset of twinning in metals: a constitutive description. Acta mater. 49, 4025–4039.
Miura, S., Takamura, J., Narita, N., 1968. Orientation dependence of flow stress for twinning in silver crystals, transactions of the Japan Institute of Metals. In: JAPAN INST METALS AOBA ARAMAKI, SENDAI 980, JAPAN, p. 555.
Müllner, P., Romanov, A., 2000. Internal twinning in deformation twinning. Acta mater. 48, 2323–2337.
Nabarro, F., 1947. Dislocations in a simple cubic lattice. Proc. Phys. Soc. 59, 256.
Neuhäuser, H., Schwink, C., 1993. Solid solution strengthening. Mater. Sci. Technol. 193–250.
Neumann, P., 1986. Low energy dislocation configurations: a possible key to the understanding of fatigue. Mater. Sci. Eng. 81, 465–475.
Nishizawa, T., Ishida, K., 1983. The Co– Ni (Cobalt-Nickel) system. Bull. Alloy Phase Diagrams 4, 390–395.
Ogata, S., Li, J., Yip, S., 2002. Ideal pure shear strength of aluminum and copper. Science 298, 807–811.
Paul, H., Driver, J.H., Maurice, C., Piątkowski, A., 2007. The role of shear banding on deformation texture in low stacking fault energy metals as characterized on model Ag crystals. Acta mater. 55, 575–588.
Paul, H., Morawiec, A., Driver, J.H., Bouzy, E., 2009. On twinning and shear banding in a Cu–8at.% Al alloy plane strain compressed at 77K. Int. J. Plasticity 25, 1588–1608.
Peierls, R., 1940. The size of a dislocation. Proc. Phys. Soc. 52, 34.
Pfeiler, W., 2008. Alloy physics: a Comprehensive Reference. John Wiley & Sons.
Pirouz, P., 1989. On twinning and polymorphic transformations in compound semiconductors. Scr. Metall. 23, 401–406.
Remy, L., 1978. Kinetics of fcc deformation twinning and its relationship to stress-strain behaviour. Acta Metall. 26, 443–451.
Robertson, I.M., 1986. Microtwin formation in deformed nickel. Philosophical Magazine a: physics of condensed matter, structure. Defects Mech. Prop. 54, 821–835.
Salehinia, I., Bahr, D., 2014. Crystal orientation effect on dislocation nucleation and multiplication in FCC single crystal under uniaxial loading. Int. J. Plasticity 52, 133–146.
Schoeck, G., 1994. The generalized Peierls–Nabarro model. Philos. Mag. A 69, 1085–1095.
Schoeck, G., 2005. The Peierls model: progress and limitations. Mater. Sci. Eng. A 400, 7–17.
Shin, I., Carter, E.A., 2014. Simulations of dislocation mobility in Magnesium from first principles. Int. J. Plasticity 60, 58–70.
Skoczeń, B., Bielski, J., Sgobba, S., Marcinek, D., 2010. Constitutive model of discontinuous plastic flow at cryogenic temperatures. Int. J. Plasticity 26, 1659–1679.
Sleeswyk, A., 1963. ½< 111> screw dislocations and the nucleation of {112}< 111> twins in the bcc lattice. Philos. Mag. 8, 1467–1486.
Smallman, R.E., Bishop, R.J., 1999. Modern Physical Metallurgy and Materials Engineering. Butterworth-Heinemann.
Smith, W.F., 1993. Structure and Properties of Engineering Alloys.
Suzuki, H., 1962. Segregation of solute atoms to stacking faults. J. Phys. Soc. Jpn. 17, 322–325.
Tadmor, E., Bernstein, N., 2004. A first-principles measure for the twinnability of FCC metals. J. Mech. Phys. Solids 52, 2507–2519.
Tadmor, E., Hai, S., 2003. A Peierls criterion for the onset of deformation twinning at a crack tip. J. Mech. Phys. Solids 51, 765–793.
Tadmor, E.B., Miller, R.E., 2011. Modeling Materials: Continuum, Atomistic and Multiscale Techniques. Cambridge University Press.
Van Swygenhoven, H., Derlet, P., Frøseth, A., 2004. Stacking fault energies and slip in nanocrystalline metals. Nat. Mater. 3, 399–403.
Venables, J., 1964a. The electron microscopy of deformation twinning. J. Phys. Chem. Solids 25, 685–692.
Venables, J., 1964b. The nucleation and propagation of deformation twins. J. Phys. Chem. Solids 25, 693–700.
Vitek, V., 1970. On the stability of stacking faults in BCC crystals. Philos. Mag. 21, 1275–1278.
Warner, D., Curtin, W., Qu, S., 2007. Rate dependence of crack-tip processes predicts twinning trends in fcc metals. Nat. Mater. 6, 876–881.
Weston, W., Granato, A., 1975. Cubic and hexagonal single-crystal elastic constants of a cobalt-nickel alloy. Phys. Rev. B 12, 5355.
Xiao, X., Song, D., Xue, J., Chu, H., Duan, H., 2015. A size-dependent tensorial plasticity model for FCC single crystal with irradiation. Int. J. Plasticity 65, 152–167.
Xiong, L., Xu, S., McDowell, D.L., Chen, Y., 2015. Concurrent atomistic–continuum simulations of dislocation–void interactions in fcc crystals. Int. J. Plasticity 65, 33–42.